ELECTROCHEMICAL PROPERTIES OF TITANIA BASED POWDERS

A Thesis Submitted to
the Graduate School of Engineering and Sciences of
İzmir Institute of Technology
in Partial Fulfillment of the Requirements for the Degree of

MASTER OF SCIENCE

in Materials Science and Engineering

by
Cem TÜRKAY

October, 2015
İZMİR

We approve the thesis of **Cem TÜRKAY**

Examining Committee Members:

_____

Prof. Dr. Mustafa M. DEMİR
Department of Materials Science and Engineering, Izmir Institute of Technology

_____

Assist. Prof. Dr. Engin KARABUDAK
Department of Chemistry, Izmir Institute of Technology

_____

Assist. Prof. Dr. Nesrin HORZUM POLAT
Department of Bio Engineering Sciences, Izmir Katip Çelebi University

27 October 2015

_____

Prof. Dr. Mustafa M. DEMİR
Supervisor, Department of Materials Science and Engineering, İzmir Institute of Technology

_____

Prof. Dr. Mustafa M. DEMİR
Head of the Department of Materials Science and Engineering

_____

Prof. Dr. Bilge KARAÇALI
Dean of the Graduate School of Engineering and Sciences

ACKNOWLEDGEMENTS

Firstly, I would like to thank my supervisor Prof. Dr. Mustafa M. DEMİR for letting possibility to complete this thesis and helping during my M.S. studies. I would like to say my special thanks to my co-advisor Prof. Dr. Muhsin ÇİFTÇİOĞLU for encouragement, his instructive guidance. Furthermore, my special thanks go to, Dr. Sema DEMİRCİ UZUN and Dr. Arda YURTSEVER because of their technical and academic help.

In addition, I am indebted to the thesis committee members Assist. Prof. Dr. Engin KARABUDAK and Assist. Prof. Dr. Nesrin HORZUM POLAT for their valuable comments on my thesis.

I would also like to acknowledge to Adnan TAŞDEMİR and Tuğçe SEMERCİ for their infinite encouragement and hardworking personalities. I would also like to state my deepest thanks to Kenan Yılmaz, Öncel Kırkbaş and Kaan Yaltrık who helped me during my thesis for their friendship and support whenever I needed.

Finally, I can’t find better words to explain the contribution of my family to my education and explain their love. I express my thanks for their helps.

ABSTRACT

ELECTROCHEMICAL PROPERTIES OF TITANIA BASED POWDER

Global warming arising from the greenhouse effect is globally accepted as the main problem which may threaten the life on the earth. Excess emission of carbon dioxide which leads to the more absorption of solar radiation in the atmosphere is the main reason for global warming. Carbon dioxide present in the atmosphere is balanced by natural photosynthesis; however this balance was disturbed by the increasing amount of carbon dioxide emissions after industrial revolution. Intense efforts was made by many scientists to find solutions to decrease the carbon dioxide level in the atmosphere and the pioneering studies were conducted in the early 1970s which founded the basic theory of artificial photosynthesis.

The conceptual idea on conducting photosynthesis by technologically feasible processes was accepted by many scientists and the research on artificial photosynthesis accelerated in the last 10 years. The enhancement of the efficieny of artificial photosynthesis, by which alternative fuels such as methane, methanol may be produced, can be realized by doping titanium dioxide which is the most widely used photocatalyst in the literature. The determination of new electrochemical properties obtained by doping titanium dioxide is crucial since the oxidation/reduction reactions are controlled by the electrochemical structure of this material. Bandgap and band position energy levels which are important properties in photocatalysis can be determined and the efficiency of photoreduction under UV or visible light corresponding to these energy levels can be improved. Cyclic voltammetry (CV) can be used to determine the electrochemical properties of titanium dioxide and these properties can be improved by using the information obtained with this method.

The effects of rare earth element doping on the electrochemical properties of titanium dioxide were investigated through out this Msc study. It was found that doping of titanium dioxide is significantly increased the electrochemical activity with rare earth elements. The increase in the doping amount of elements showed that articial photosynthesis activity of titanium dioxide may be enhanced by rare earth element doping.

ÖZET

TİTANYUMDİOKSİT TEMELLİ TOZLARIN ELEKTROKİMYASAL ÖZELLİKLERİ

Günümüzde insanlığın varlığını tehdit edebilecek en büyük problemlerden birinin sera gazı efektine bağlı olarak ortaya çıkan küresel ısınma olduğu kabul görmektedir. Bu durumun temel sebebi karbondioksit gazının aşırı salınımı ve sonucunda da güneş ışınlarının atmosferde daha fazla emilmesidir. Karbondioksit gazı hep vardı ve fotosentez tarafından dengeleniyordu ancak sanayi devriminden sonra bu gazın salımı öyle arttı ki biliminsanları bu konuda çözüm üretmek için çalışmaya başladılar ve ilk defa 1970 lerde yapay fotosentez kavramına temel oluşturan yayınlar yapıldı.

Fotosentezin canlılara değil de aygıtlara yaptırılması fikri birçok biliminsanı tarafından kabul gördü ve bu çalışmalar özellikle son 10 yılda hız kazandı. Bu noktada, metan, metanol gibi alterneatif yakıtların üretildiği yapay fotosentezdeki aktivitenin artırılması için literatürde en yaygın kullanılan fotokatalizör olan titanyum dioksitin katkılanması ve katkı ile elde edilen yeni elektrokimyasal özelliklerin saptanması büyük bir öneme sahiptir. Bu sayede fotokatilizde büyük öneme sahip olan bant genişliği ve bant pozisyonu enerji seviyeleri net bir şekilde belirlenebilir ve bu enerji seviyelerine denk gelen UV veya görünür ışık altında fotonik indirgenme verimleri iyileştirebilir. Titanyum dioksitin elektrokimyasal özellikleri döngüsel gerilimölçer (cyclic voltammetery – CV) yöntemi ile araştırılabilir ve bu özelliklerin iyileştirilmesine yönelik kullanılabilecek bulgular bu yöntem sayesinde üretilebilir.

Bu tez çalışmasında nadir toprak elementi katkısının titanyum dioksitin elektrokimyasal özellikleri üzerindeki etkisi incelenmiştir. Nadir toprak elementi katkısının titanyum dioksitin elektriksel aktifliğini önemli ölçüde artırdığı bulunmuştur. Bu bağlamda titanyum dioksitin yapay fotosentezdeki aktivitesinin nadir toprak elementi katkısı ile artırabileceğini gösterilmiştir.

To my Family

TABLES OF CONTENTS

LIST OF TABLES viii

LIST OF FIGURES ix

CHAPTER 1. INTRODUCTION 1

CHAPTER 2. PHOTOREDUCTION 4

2.1. General Information 4

2.2. Photosynthesis 4

2.3. CO_2 Photoreduction Mechanism 7

2.4. Photocatalysts 8

2.4.1. Titanium dioxide 13

2.4.2. Sol-Gel Method 17

2.5. Valence – Conduction Band 18

2.5.1. Oxidation Reduction Reactions 21

2.5.2. Cyclic Voltammetry 23

CHAPTER 3. EXPERIMENTAL 33

3.1. Preparation of the Films 33

3.2. Characterization of the Films 38

3.3. CV Measurements 38

CHAPTER 4. RESULTS AND DISCUSSION 41

4.1. Characterization of the Powders and Sols 41

4.2. Characterization of the Films 43

4.3. CV Measurements 46

CHAPTER 5. CONCLUSION 61

REFERENCES 62

LIST OF FIGURES

Figure **Page**

Figure 1.1. Energy demand 1
Figure 2.1. Coupled water splitting and CO_2 reduction 4
Figure 2.2. The Calvin cycle.....5
Figure 2.3. Life an earth with a CO_2 cycle 6
Figure 2.4. (a) Photocatalytic water splitting (b) Surface reactions..... 8
Figure 2.5. Schematic of photoexcitation of a semiconductor..... 9
Figure 2.6. Mechanism of water splitting on a photo-activated semiconductor.....10
Figure 2.7. Relationship between band structure of semiconductor and redox potentials of water splitting 11
Figure 2.8. Applications of semiconducting materials 12
Figure 2.9. The variation of nanomaterials investigated for photocatalytic hydrogen production in literature 12
Figure 2.10. a) Rutile b) Anatase form of crystals of TiO_2 13
Figure 2.11. Crystal structures form of TiO_2 (from left to right: rutile, brookite, anatase) 14
Figure 2.12. Applications of TiO_2 16
Figure 2.13. A schematic view of a solar cell 16
Figure 2.14. The Band – Gap concept 18
Figure 2.15. Basic Instruments of Electrochemistry 19
Figure 2.16. Reduction processes and potentials 20
Figure 2.17. An Electrochemical Cell.....20
Figure 2.18. Oxidation and Reduction 21
Figure 2.19. Applied Potential in Cylic Voltammetry 23
Figure 2.20. An Ideal Voltammogram 25
Figure 2.21. Electrochemical interactions of a typical voltammogram onto regional base.....26
Figure 2.22. The schematic illustration of the CV system fundamentally, is working with electrolyte solution as expected 27
Figure 2.23. The schematic illustration of a typical CV (a) CV and (b) multiple CV of modified GCE in 0.1 M of KCl solution, MB is methylene blue 28

Figure 2.24. The existance or non existance of cyclic voltammograms and peaks (a) After photoreaction and (b) before photoreaction for 0.4 wt%CoO$x$$TiO_2$ electrodes before and after photoreaction with illumination Solution: 0.1 mol Na_2SO_4, Scan rate, 50mVs−1..... 29
Figure 2.25. Cyclic voltammetry curves recorded for doped and pristine TiO_2 , immersed in 0.1 M K_2SO_4, at a scan rate 50 mV/s.....30
Figure 2.26. Cyclic voltammetry curves for variously prepared TiO_2 samples Electrochemical properties of novel titania nanostructures 31
Figure 2.27. (a) Voltammograms of PGTNs, PTNs and TiO_2 at 5 mV. (b–c) CV curves of PGTNs and PTNs at different scan rates. (d) Square roots of various scan rates (v1/2) vs. Oxidation peak current (Ip) 32
Figure 3.1. A schematic representation of REE doped sol-gel TiO_2 powder preparation process 34
Figure 3.2. TiO_2 film coated ITO glasses prepared by doctor-blade technique……. 35
Figure 3.3. Colour Change of Titania Powders 35
Figure 3.4. Image of cerium doped TiO_2 sol.....36
Figure 3.5. Drying the Sticks 37
Figure 3.6. TiO_2 coated titanium sticks ……..37
Figure 3.7. Three-electrode cell for CV measurements ……..... 39
Figure 3.8. Experimental setup for CV measurements ……...39
Figure 3.9. N_2 purging of 0.1 M KCl solution .....
Figure 4.1. XRD patterns of the prepared powders ……41
Figure 4.2.
Figure 4.3. Bare titanium stick 43
Figure 4.4. Ce doped TiO_2 coated titanium stick 44
Figure 4.5. SEM images of the bare titanium sticks 45
Figure 4.6. SEM images of Nb doped TiO_2 film coated titanium sticks 45
Figure 4.7. CV voltagram of bare titanium stick 47
Figure 4.8. CV voltagram of 0.25% Nd doped TiO_2 coated titanium wire 48
Figure 4.9. CV voltagram of 0.5% Nd doped TiO_2 coated titanium wire 49
Figure 4.10. CV voltagram of 1% Nd doped TiO_2 coated titanium wire 50
Figure 4.11. CV voltagram of 2% Nd doped TiO_2 coated titanium wire 51
Figure 4.12. CV voltagram of 2% Er doped TiO_2 coated titanium wire 52
Figure 4.13. CV voltagram of 5% Er doped TiO_2 coated titanium wire 53

Figure 4.14. CV voltagram of 5% Ce doped TiO_2 coated titanium wire 54
Figure 4.15. CV voltagram of 5% La doped TiO_2 coated titanium wire 55
Figure 4.16. CV voltagram of 5% Ce doped TiO_2 coated titanium wire 56
Figure 4.17. Voltammograms of Pristine TiO_2 with various scan rates 57
Figure 4.18. Voltammograms of 0.5 Nd doped TiO_2 with various scan rates.....58
Figure 4.19. Voltammograms of % 1 Ce, La and Nd doped TiO_2 samples 59
Figure 4.20. Voltammograms of pure TiO_2 samples with 50mV/s and 70mV/s to compare surface areas of single and pair wires.....60

LIST OF TABLES

Table **Page**

Table 2.1. Lattice parameters, bond lengths and angles of anatase and rutile..... 14

Table 2.2. Sample structures and calculated specific capacitances.....31

Table 4.1. Experimental conditions. 46

CHAPTER 1

INTRODUCTION

Recent research have focused on generating renewable energy sources due to the problems arising from the usage of conventional fossil fuels (Figure 1.1). Anthropogenic CO_2 emissions increased due to the increasing fossil fuel use since the beginning of industrial revolution and the excess CO_2 which cannot be consumed by the plants started to accumulate in the atmosphere. This accumulated CO_2 and other chlorofluorohydrocarbons in the atmosphere caused what is known as "Greenhouse Effect" phenomenon and global warming.

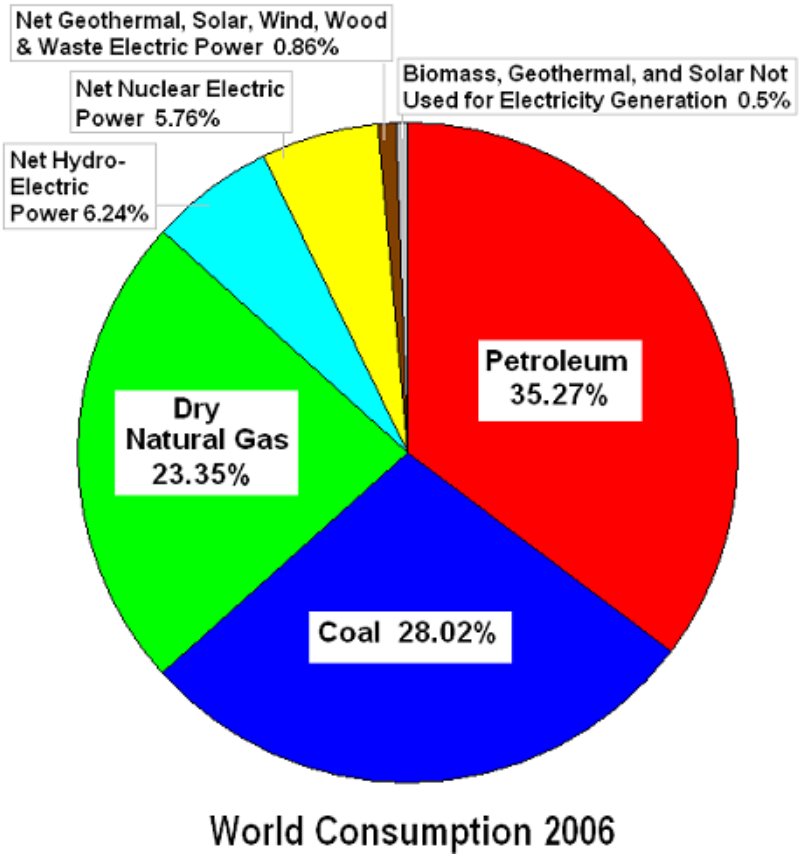

Figure 1.1.Energy demand
(Source: World Consumption, 2006)

Up to 17th century, plants balanced the amount of CO_2 by photosynthesis. Now the natural photosynthesis activity is not sufficient for maintaining the CO_2 balance and searching alternatives seems essential. The aim should be not only reducing CO_2 and chlorofluorohydrocarbon levels in the atmosphere, but also forming new organic molecules such as methane that can be used as an energy source. Research on the utilization of solar energy in order to satisfy the increasing energy demand and to decrease the "Greenhouse Effect" gained significant interest in the last couple of decades. Artificial photosynthesis is being considered as a promising technique for the synthesis of renewable, sustainable fuels like methane, methanol and hydrogen and the reduction of the global CO_2 content in the environment (Cogdell et al. 2010). This phenomenon is based on the use of a photocatalyst which is a semiconductor activated by sunlight energy and triggers the reactions including water splitting and CO_2 reduction.

Photocatalyst materials play a central role in the success of the photocatalytic processes and artificial photosynthesis. These materials should be corrosion resistant (Zhu and Zach 2009), chemically stable and cheap with high and efficient visible light absorption (Silija et al. 2012). The commonly known anatase and rutile phases of titania (TiO_2) are the most important and widely used materials in environmental related photocatalytic research and applications. The most important disadvantage of these titania phases is their relatively high bandgap energies commonly reported in the 3.0-3.2 eV range which results in the very limited absorption of sun light in the ultra-violet (UV) range which represents < 5% of solar radiation spectrum (Nassoko et al. 2012). The reduction and modification of the bandgap energies of the titania phases by doping with various elements for more efficient absorption in the visible range and the determination of the activities of these materials in the photocatalytic decomposition of organic structures and artificial photosynthesis is the main concern of intense research in the last 10-15 years. These dopants are nonmetals like C, N, S etc. (Cong et al. 2007, Dong et al. 2011, Park et al. 2006, Rockafellow et al. 2009, Shen et al. 2007, Yang et al. 2010) transition metals like Cu, Ag, Fe, Co etc. (Akpan and Hameed 2010, Silija et al. 2012, Baiju et al. 2007, Nie et al. 2009) and rare earth metals like La, Ce, Nd etc. (Choudhury et al. 2013, Li et al. 2004, Obregon et al. 2013, Ranjit et al. 2001, Xiao et al. 2007).

In this thesis, band position energy levels which determine the oxidation/reduction reactions in artificial photosynthesis were determined by using Cyclic Voltammetry (CV) which is preferred due to its working capability even in nanoamper levels. The effects of

rare earth element type, doping level, electrolyte type, electrolyte concentration on the electrochemical behavior of TiO_2 were investigated in this MSc study.

CHAPTER 2

PHOTOREDUCTION

2.1. General Information

Photoreduction is a chemical process that is carried out by the species formed by the electron-hole pairs generated due to the interaction of light and the semiconductor. Photoreduction is used to represent the reaction which is induced by light and it generally outputs photoexcited species or photochemical hydrogenation of a molecule by the addition of one or more electrons. The photoreduction of CO_2 and water splitting have been widely studied for years. The reactions are shown in Figure 2.1.

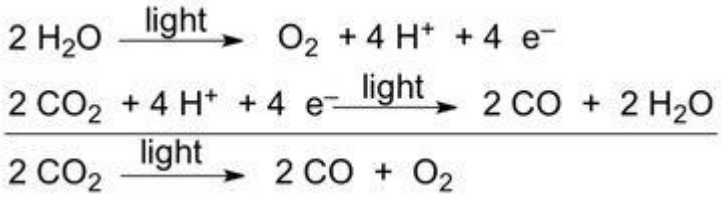

Figure 2.1. Coupled water splitting and CO_2 reduction
(Source: Electrochemical photoreduction, 2015)

2.2. Photosynthesis

In natural photosynthesis plants and cyanobacteria synthesize their own building block materials from CO_2 with the help of sunlight energy. Photon energy splits water into oxygen and hydrogen which is then bounded to NADPH (Nicotinamide adenine dinucleotide phosphate). This process, which is called as *Light Reactions*, is conducted at photosynthesis reaction centers embedded in cell wall and includes the electron transfer related to ATP (Adenozine triphosphate) synthesis. In *Dark Reactions*, NADPH, ATP and CO_2 is consumed in Calvin Cycle (Figure 2.2) to produce carbohydrates (Heldt 2005).

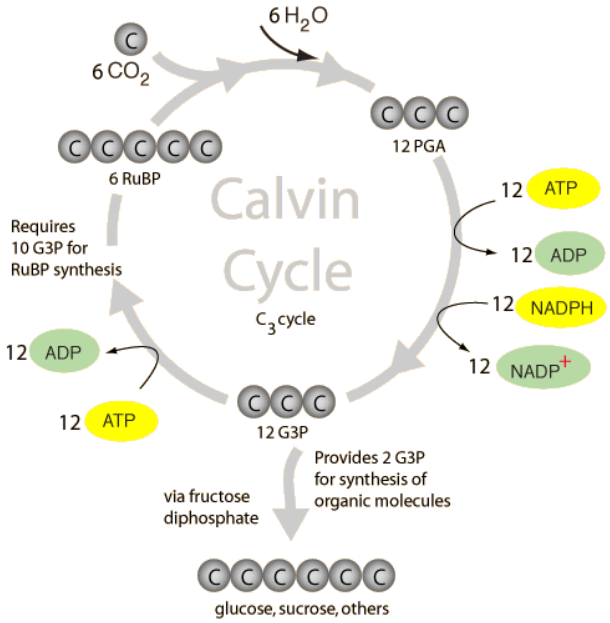

Figure 2.2. The Calvin Cycle
(Source: Moore et al. 1995)

Plants and cyanobacteria are important due to their capability of producing biomass, oxygen and all fossil fuels by photosynthesis. The CO_2 cycle and photosynthesis phenomena (Figure 2.3) are the vital living processes in human life and the whole organics cycles. Animals need carbohydrates or other organics for the continuity of their life so their existance. These animals oxidize biomass that is produced by plants or bacteria and they utilize this needed energy to continue their own life processes. In other words, solar energy is captured and used by plants and this fundamental step starts the life cycles and become the source of the life processes on earth (Heldt 2005).

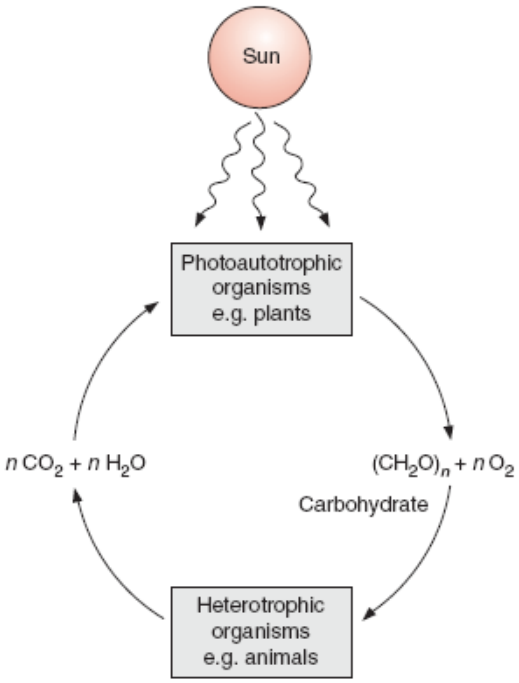

Figure 2.3. Life on Earth with a CO_2 cycle
(Source: Heldt, 2005)

The light coming from sun has a broad range of wavelength (λ) containing three main regions which are ultraviolet (UV and λ_{UV}< 4000 nm) visible (400 nm <$\lambda_{visible}$< 700 nm) and infrared (IR and λ_{IR}> 720 nm) and these range is thought with different energy amounts due to the Planck's equation (E=h.f) where f is the frequency of radiation. Plants absorb this energy from the sun light and this energy initiates the photosynthesis reactions in chlorophylls.

Solar energy can be utilized in many different applications. For instance this energy can be converted to electricity by solar cell or the energy can be stored by solar pond on this energy can be transformed into chemical energy by photosynthesis (Hammarstrom and Hammes-Schiffer 2009). There are several advantages/disadvanteges of these applications. Photocatalysis is supposed to create a great contribution to environmental issues by carbon emission reduction and renewable energy generation (Fujishima et al. 2000).

By using photocatalysis, harmful species from industrial wastes can be transformed into harmless disposable species. Some chemical reactions that can occur only at high temperatures and pressures may be triggered by the electrons and holes produced by the interaction of photocatalyst and sun light. In this sense, artificial photosynthesis is a promising process to produce sustainable energy to for the global

warming prevention and these all are supported by the intensive research in the last 10 years (Wu et al. 2005, Matejova et al. 2014, Raja et al. 2011, Tan et al. 2012, Uner et al. 2011, Zhang et al. 2009).

Effective use of renewable energy sources is needed to protect the environment. Photocatalysis is expected to be a promising solution to eliminate these kind of problems that may occur in the future applications. Photocatalysts materials can also be used to decompose pollutants in water, air and on reactive surfaces. There are many research conducted on several different materials towards photocatalytic water splitting and artificial photosynthesis in the last decade (Dey 2007, Fan et al. 2009, Inoue 2009, Kalyanasundaram and Graetzel 2010, Neatu et al. 2014, de-Richter et al. 2013, Zhu and Zach 2009). During all the achievements, "Artificial Photosynthesis Center" was built in California, USA and this center has a budget of 120 million $. This center is supporting many universities and national laboratories working on artificial photosynthesis (Subbaraman 2010).

2.3. CO_2 Photoreduction Mechanism

Photoreduction mechanism of CO_2 includes water splitting and reduction of CO_2 with species formed in water splitting reactions. This whole process is demonstrated step by step schematically in Figure 2.4. The properties such as the capability of absorption of photons, charge separation/migration and surface adsorption/reactions of a semiconducting photocatalyst determine the important steps in photocatalysis.

Photocatalysis involves oxidation and reduction reactions due to photogenerated holes and electrons. When water is adsorbed on the surface of the semiconducting material, it produces O_2 and H^+ due to the reaction of captured holes with water. Produced H^+ ions react with excited electrons to form H· radicals. On the other hand, one H_2 molecule forms by union of two H· radicals. The photocatalytic water splitting mechanism can be simply expressed by these two steps. When an electron interact with CO_2 molecule, $\cdot CO_2^-$ radical is formed (Koci et al. 2009). CO is formed by the reaction of newly formed H· and $\cdot CO_2^-$ radical. By consecutive reactions, CO is transformed into $\cdot CH_3$ radicals. As followings, by the reaction of $\cdot CH_3$ radicals with H· or OH· radicals, CH_4 (methane) or CH_3OH (methanol) molecules are formed. The photocatalytic reduction mechanism of CO_2 is explained by these steps. The heat is released without

chemical works due to the recombination of produced electron-hole pairs which is not desired in photocatalysis.

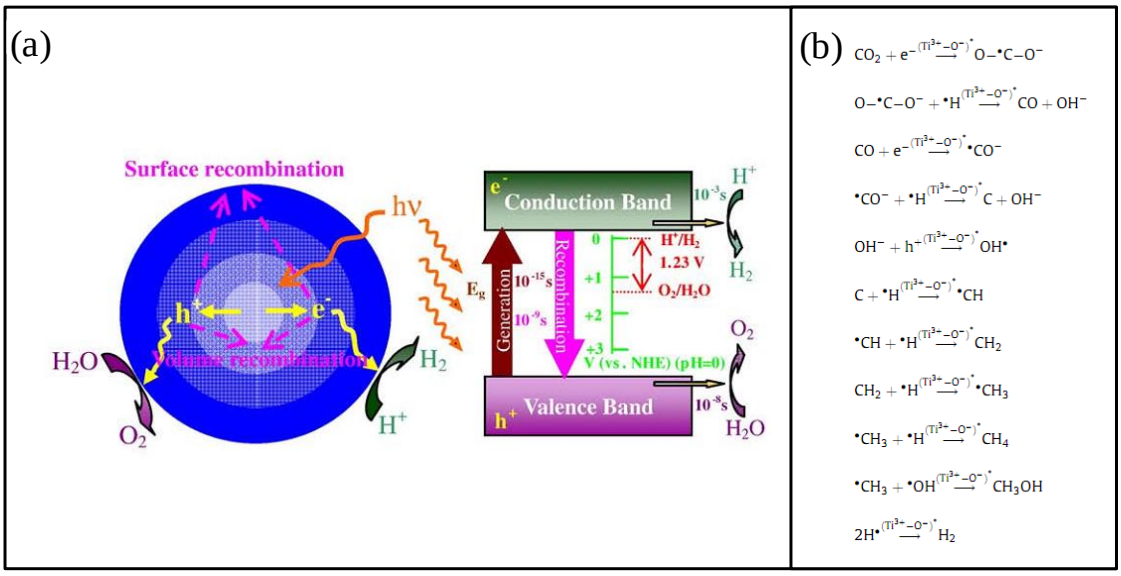

Figure 2.4. (a) Photocatalytic Water Splitting (b) Surface Reactions
(Source: Koci et al. 2009, Zhu and Zach. 2009)

2.4. Photocatalysts

Photocatalysts are generally semiconductors (mostly metal oxides) with a bandgap energy (Eg) between valence and conduction bands. The activation of semiconductor photocatalyst is supplied by exposing these materials to light which incoming photons have energies equal to or higher than the bandgap energy of that material (Figure 2.5). When the semiconductor is excited, an electron (e^-) hops from the valence band to the conduction band and a hole is created in the valence band which acts as a positively charged electron (Linsebigler et al. 1995).

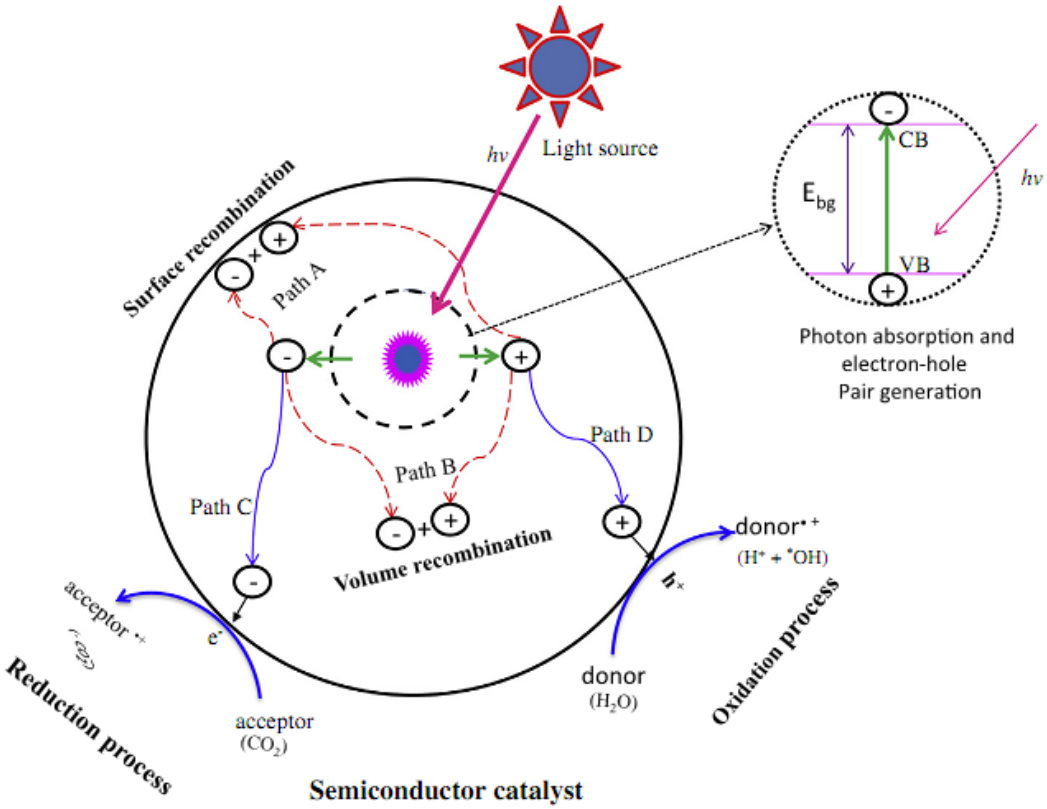

Figure 2.5. Schematic of Photoexcitation of a Semiconductor
(Source: Tahir and Amin, 2013)

When a semiconductor has properties such as (i) photoactivity, (ii) biologically and chemically inert; (iii) photostable (i.e., not prone to photocorrosion), (iv) inexpensive and (v) non-toxic, it can be classified as an ideal photocatalyst. There are several processes occuring after absorption of light by a photocatalyst. Firstly, by energy transfer from the absorbed photons to the semiconductor electrons hop from the valence band to the conduction band leaving holes acting as positively charged electrons. Excited electrons and holes can recombine dissipating the input energy as heat, get trapped in metastable surface states or react with electron donors/acceptors adsorbed on or near the semiconductor surface leading to oxidation-reduction reactions (Zaleska 2008). In path A or B, electron-hole pairs are produced in the lattice and they are separated and captured in suitable parts of the nanostructure. The oxidation reactions are conducted by holes in path D and reduction reactions are conducted by electrons in path C (Linsebigler et al. 1995). The electron excitation mechanism becomes more efficient if the reactant molecules are preadsorbed on the surface of the photocatalyst. The band edge position of the semiconducting material determines the probability and the rate of charge transfer

process. The redox potential of the adsorbed species is also important for the efficiency of the photocatalytic process. The bottom of conduction band of the semiconductor must be at a more negative potential than H^+/H_2 (0 V vs. NHE at pH 0) and the top of the valence band must be at a more positive potential than H_2O/O_2 (1.23 V vs. NHE at pH 0) (Figure 2.6). The minimum electron energy should be 1.23 eV (corresponding wavelength c.a. 1000 nm) for water splitting reaction to be thermodynamically possible (Zang 2011). Some examples of photocatalysts and redox potentials of water splitting are also given in Figure 2.7.

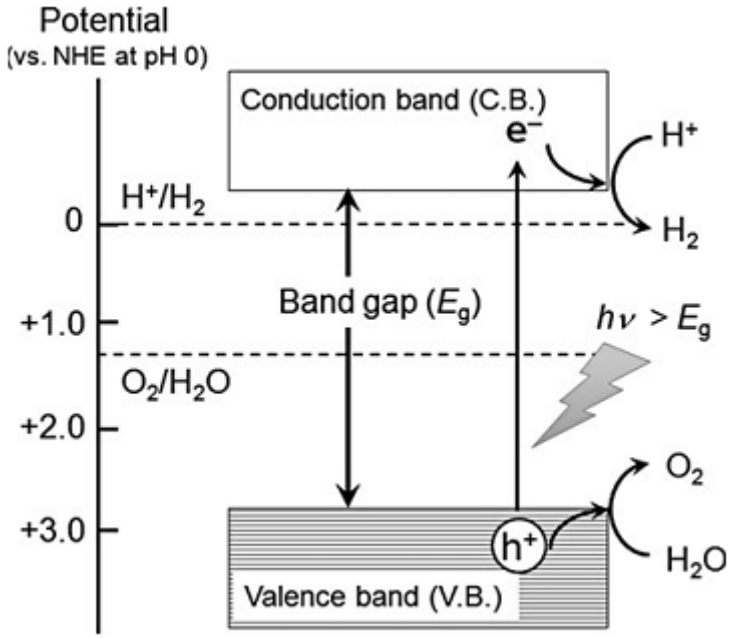

Figure 2.6. Mechanism of Water Splitting on a Photo-activated Semiconductor (Source: Zang 2011)

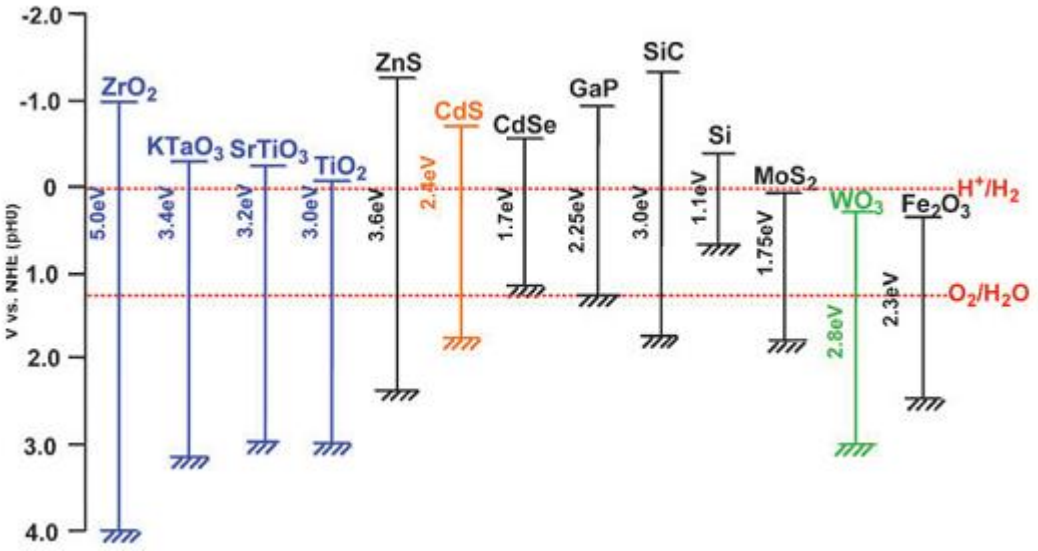

Figure 2.7. Relationship Between Band Structure of Semiconductor and Redox Potentials of Water Splitting (Source: Kudo and Miseki 2008)

Fujishima and Honda conducted the pioneering studies in the early 1970s to produce renewable energy in terms of artificial photosynthesis and water splitting by photocatalytic processes (Fujishima et al. 1972, Inoue et al. 1979). As a result of these achievements, photocatalytic processes are being conducted by various photocatalytic materials. Several materials were also commercialized by using these photocatalytic materials in the literature.

Many oxide, sulfide, nitride based semiconducting materials are employed as photocatalysts due to their suitable band gap energies for photocatalysis. TiO_2, WO_3, $SrTiO_3$, Fe_2O_3, ZnO, CuO, ZnS, CdS, CdSe, GaN are some examples for photocatalysts. The band gap energies of these materials are 3.2, 2.8, 3.2, 3.1, 3.2, 1.2, 3.6, 2.4, 1.7, 3.4 eV, respectively (Hoffman et al. 1995). These semiconductors are used in many applications including photocatalysis (Figure 2.8). TiO_2 is biologically and chemically inert and stable with respect to photocorrosion and chemical corrosion and inexpensive so that it is the most extensively used photocatalyst.

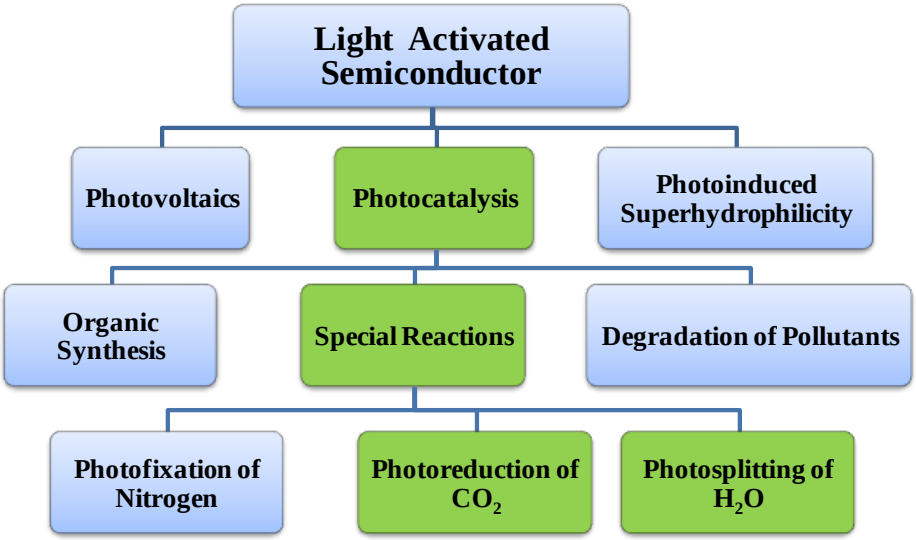

Figure 2.8. Applications of Semiconducting Materials.
(Source: Carp et al. 2004)

Semiconductor materials for CO_2 photoreduction and H_2O photosplitting have great importance because these two applications may be solutions as a convenient way to produce renewable sources and preventing global warming. Nie et al. shows the diversity of nanomaterials produced for photocatalytic hydrogen production studied in research articles published in the last 15 years as shown in Figure 2.9 (Nie et al. 2009).

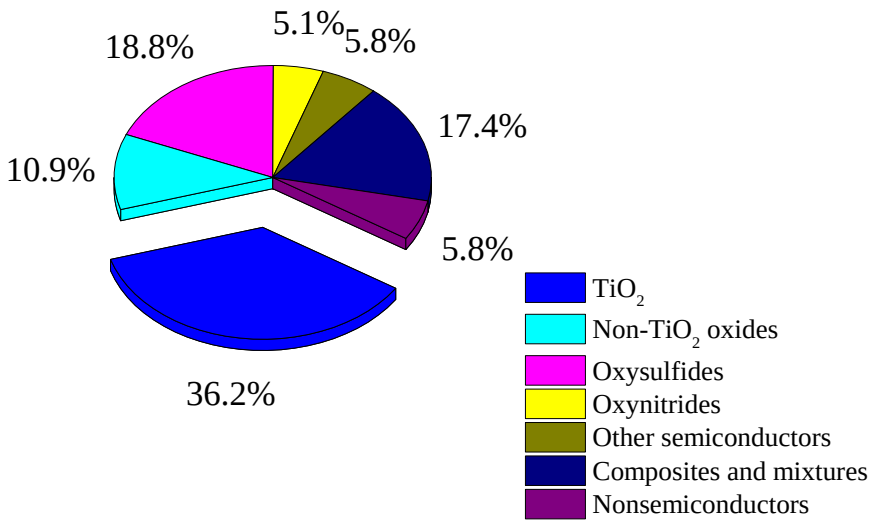

Figure 2.9. The Variation of Nanomaterials Investigated for Photocatalytic Hydrogen Production in Literature (Source: Nie et al. 2009)

2.4.1. Titanium dioxide

Titanum dioxide is a naturally occurring oxide of titanium with the chemical formula TiO_2 (Figure 2.10). It may be referred as titanium (IV) oxide, also known as titania. There are several different crystal forms of titanium dioxide such as anatase, brookite, and rutile (Figure 2.11). They are all isomers of titanium dioxide with different crystal structure. Anatase and rutile are sharing tetragonal structure, whereas brookite have an orthorhombic structure configuration. Two types are more of our interest which are anatase, rutile since they are more photocatalytically active and stable phases of titania. The lattice structures, lattice parameters and bond lengths/angles of anatase and rutile are shown in Table 2.1.

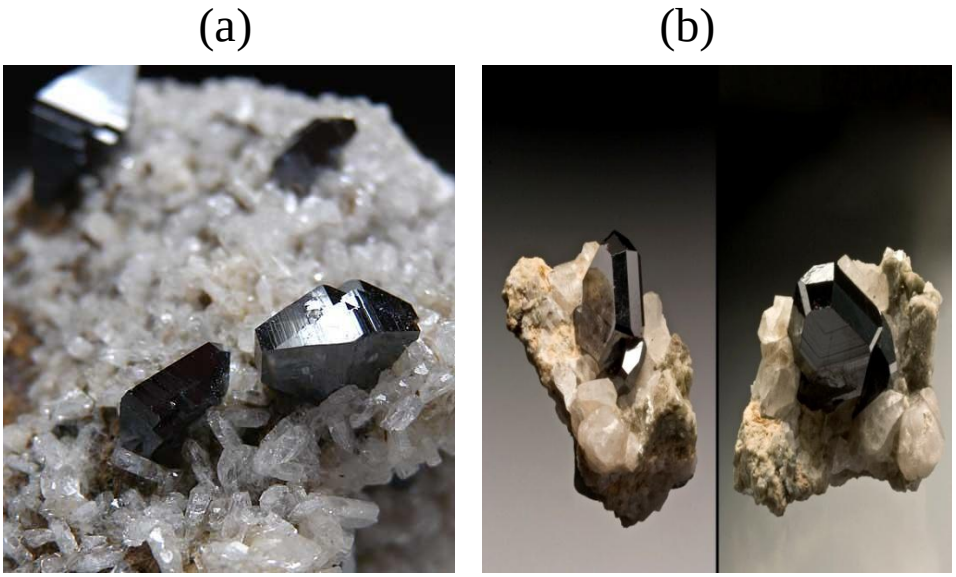

Figure 2.10. a) Rutile b) Anatase form of crystals of TiO_2
(Source: Marin Mineral, 2015; Mineral MasterPiece, 2015)

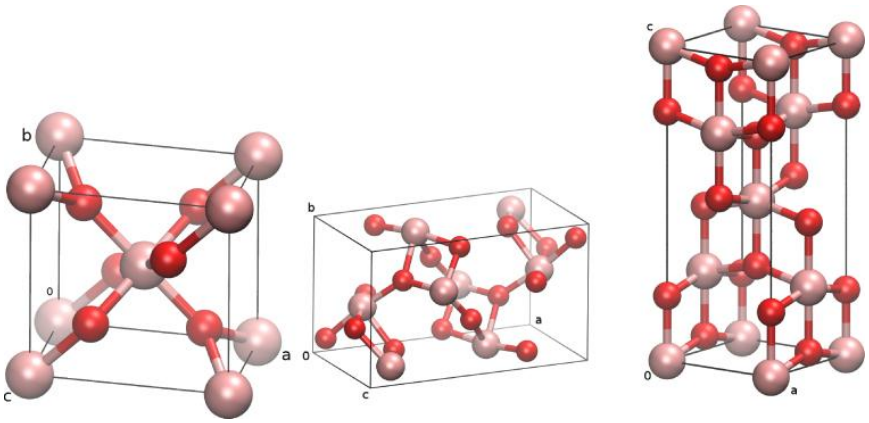

Figure 2.11. Crystal structures form of TiO_2 (from left to right: rutile, brookite, anatase) (Source: Crystal structures of titania, 2015)

Although these three types of TiO_2 have the same chemistry, they are different in crystal structure. The anatase is a crystal with small size which is isolated and somehow sharply developed. Like rutile, anatase is commonly occurring modification of TiO_2.

Table 2.1.Lattice parameters, bond lengths and angles of anatase and rutile (Source: Labouriao et al. 1997).

	Ti-O bond length (nm)	**O-Ti-O bond angle (º)**	**Lattice parameters (Å)**		
			A	b	c
Anatase	4-0.1934 2-0.1980	4-92.4 4-78.1 4-101.9	3.782	3.782	9.502
Rutile	4-0.1949 2-0.1980	2-98.8 2-81.2 8-90.0	4.594	4.594	2.958

Temperature is a very important factor which can affect their crystal structure. When they go through elevated high temperatures, then there will be structure change. We can expect anatase automatically revert to the rutile structure when the temperature goes high up to 915 º C. Unlike anatase, rutile is the more common as well as more known mineral of all those three. Anatase and rutile share many of the same or nearly the same properties, such as luster, hardness, and density. However, they differ each other slightly in crystal habit and more distinctly in cleavage due to their structure difference.

Chemical stability/inertness, low cost and absorption capability of UV light of TiO_2 make it very attractive material and it is used in research and applications of photocatalytic processes. It is widely showed in (Figure 2.12) with application types such as plastics, paper, paint and others. Excitation of one electron from the valence band to the conduction band of TiO_2 needs near UV or UV light to be absorbed due to the large band gap of TiO_2 (3.0-3.2 eV). Only UV radiation can activate TiO_2 which means no more than 5% of solar radiation may be used by TiO_2 (Carp et al. 2004). Effective use of photons of solar radiation can be achieved by using the advantages of nanoscience.

There are various application area of the titanium dioxide apart its photocatalytic properties. It is widely used as white pigment in paints owing to its high refractive index and brightness. If there are many tiny particles orientated in different directions, a high refractive index will cause the scattering of light. In other word, high refractive index means high clarity and high polarizing power. In this respect, when compared titanium dioxide to many other candidate materials. It has a higher refractive index, even higher than diamond and there are only a few other substances which also have higher index as titanium dioxides.

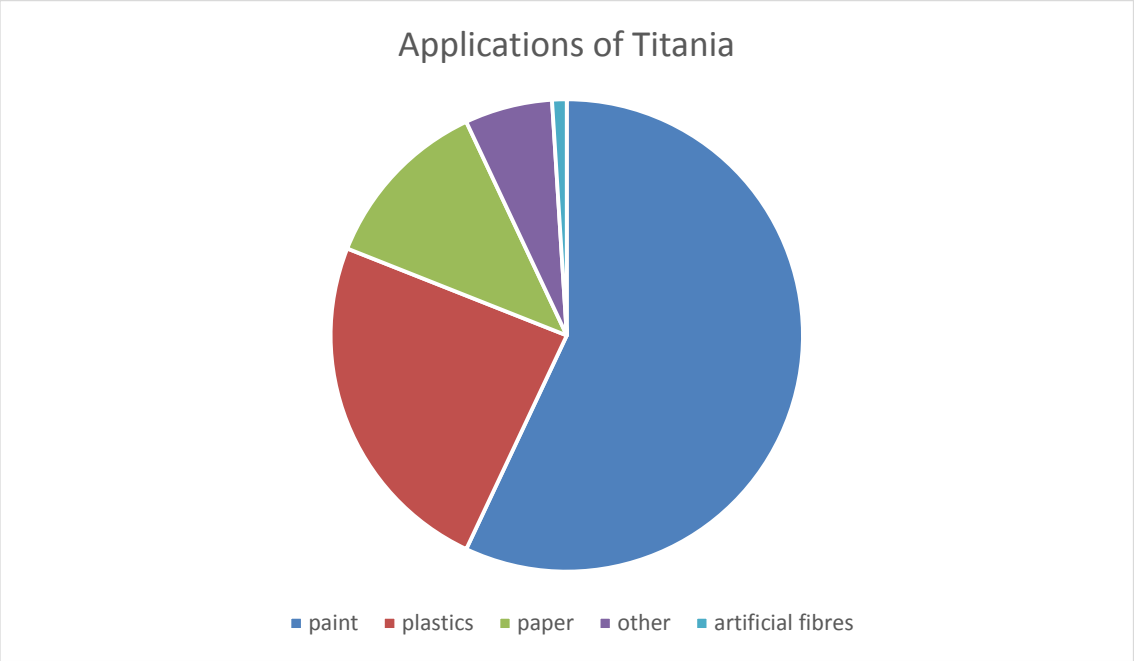

Figure 2.12. Applications of TiO_2

Considering the limited amount of available resources like fossil fuels, there is ever growing need for producing renewable energy sources in an economical way. Silicon based solar panels, which is represented in (Figure 2.13) as an example, are now widely used. But the construction of these panels need two layers of specially constructed silicon crystals. The layer structure as will be shown below is made of glass coated with conductive oxide, for example fluorine doped indium oxide which is made by adding fluorine to indium oxide and used as photo anode. The bottom layer contains nano-structured titanium dioxide.

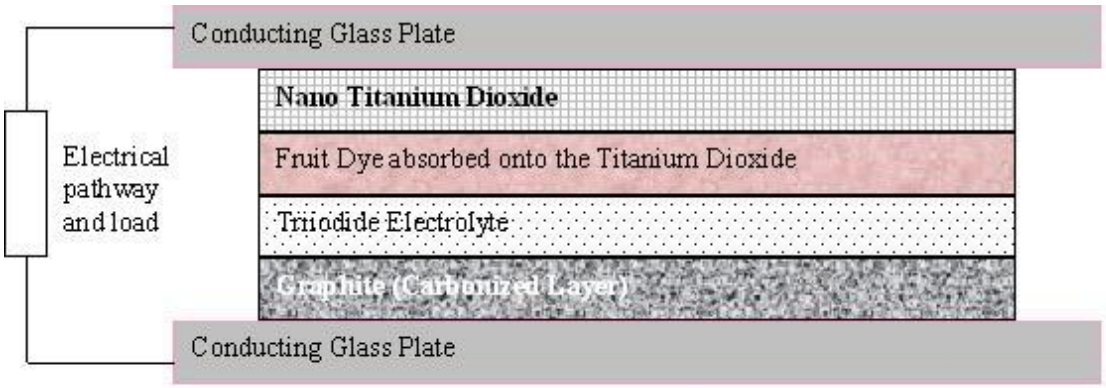

Figure 2.13.A schematic view of a solar cell
(Source: Solar cell, 2008)

2.4.2. Sol-Gel Synthesis Method

An extensive investigation in the degradation of toxic organic pollutants, in energy conversion and storage, in organic synthesis have been carried out for semiconductor as catalyst for photochemical reactions long time. In these related reactions, holes and photogenerated electrons move to the surface of semiconductor where they can induce oxidation and reduction of adsorbed molecules. Among all promising candidate for better photocatalyst, titanium dioxide, for instance, is one of the most popular in photocatalytic application because of the strong oxidizing power of its holes, also the high photostability of redox selectively bringing into the process. TiO_2 is available commercially and very easy to prepare in the laboratory. A better catalytic activity from TiO_2 can be achieved by taking a way as increasing its specific surface are, which is surely dependent on the crystal size. It is known that the catalyst in smaller size will give bigger specific surface area. So far, a couple of methods have been used to prepare TiO_2 such as chemical precipitation, microemulsion, hydrothermal crystallization and sol-gel.

For preparing metal oxides with high photocatalytic activities, sol-gel is one of the most promising techniques. In sol-gel processes, a reaction of hydrolysis and polycondensation of titanium alkoxide $Ti(OR)_n$ to form oxopolymers is usually taken place, which are then transformed into an oxide network. The reactions are as follows:

Hydrolysis reactions;

$M(OR)_4 + H_2O \rightarrow HO\text{-}M(OR)_3 + R\text{-}OH$ (partial hydrolysis)
$M(OR)_4 + 2H_2O \rightarrow (OR)_2\text{–}M\text{-}(OH)_2 + 2R\text{-}OH$ (partial hydrolysis)
$M(OR)_4 + 3H_2O \rightarrow (OR)\text{–}M\text{-}(OH)_3 + 3R\text{-}OH$ (partial hydrolysis)
$M(OR)_4 + 4H_2O \rightarrow M(OH)_4 + 4R\text{-}OH$ (total hydrolysis)

Condensation reactions;

$(OR)_3\text{–}M\text{-}OH + HO\text{–}M\text{-}(OR)_3 \rightarrow [(OR)_3M\text{–}O\text{–}M(OR)_3] + H\text{-}O\text{-}H$
$(OR)_3\text{–}M\text{-}OR + HO\text{–}M\text{-}(OR)_3 \rightarrow [(OR)_3M\text{–}O\text{–}M(OR)_3] + R\text{-}OH$

Sol-gel method has couple of advantages over other known methods. It give high purity and homogenous product, excellent atomic mixing, low temperature synthesis, precise control of size and surface properties, possibility of different forms of products such as films or powders. However high amount of solvent usage is the most important drawback of sol-gel method.

2.5. Valence – Conduction Band

A free electron is assumed to stand almost everywhere in an atom. However, Quantum Mechanics predict specific and discrete energy levels electron can only stay due to the interaction between the electron and nucleus. This phenomena is experimentally defined as valence band, conduction band and energy gap (Figure 2.14). These terms are used to show how much energy is needed for conductivity.

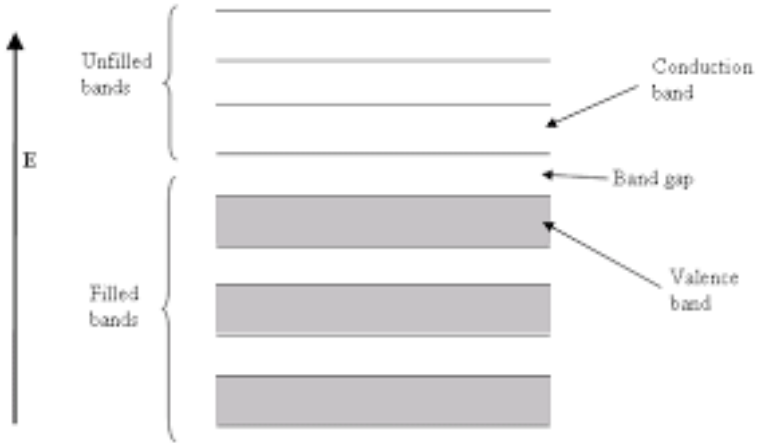

Figure 2.14.The Band – Gap concept Electrochemistry

Electrochemistry is a concept which deals with the interrelation of electrical and chemical effects. Reactions occur due to the involving reactant: electron. When the current moves throughout the molecules, chemical changes form and stability breaks which can be thought in (Figure 2.15). Thus, this area is thought to analyze and charecterize the electrical properties of coated material as. This phenomena was developed by Volta in 1793 firstly, which could form oxygen and hydrogen gases from pure water.

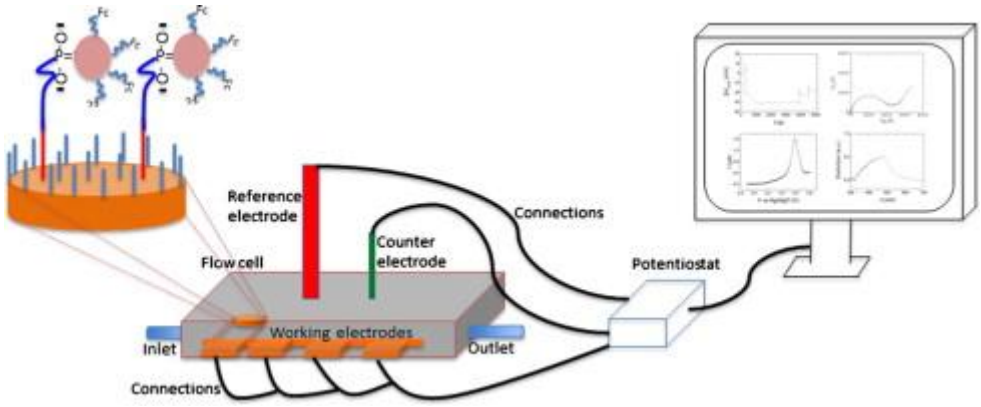

Figure 2.15. Basic Instruments of Electrochemistry (Source: Nello Formisano et al.)

Combination of chemical and electrical effects bring about lots of special characterization techniques which can lead enhancements in nanotechnologhy, chemistry and materials sciences. There are two main types of applications;

1- Electrolytic process: Reactions in which chemical changes occur on the passage of an electrical current
2- Voltaic process: Chemical reactions that result in the production of electrical energy.

Both are tested in an electrochemical cells. In Figure 2.16 lots of half reaction processes and potentials are listed respectively.

Table 17.1 Standard Reduction Potentials at 25°C (298 K) for Many Common Half-Reactions

Half-Reaction	$E°$ (V)	*Half-Reaction*	$E°$ (V)
$F_2 + 2e^- \rightarrow 2F^-$	2.87	$O_2 + 2H_2O + 4e^- \rightarrow 4OH^-$	0.40
$Ag^{2+} + e^- \rightarrow Ag^+$	1.99	$Cu^{2+} + 2e^- \rightarrow Cu$	0.34
$Co^{3+} + e^- \rightarrow Co^{2+}$	1.82	$Hg_2Cl_2 + 2e^- \rightarrow 2Hg + 2Cl^-$	0.27
$H_2O_2 + 2H^+ + 2e^- \rightarrow 2H_2O$	1.78	$AgCl + e^- \rightarrow Ag + Cl^-$	0.22
$Ce^{4+} + e^- \rightarrow Ce^{3+}$	1.70	$SO_4^{2-} + 4H^+ + 2e^- \rightarrow H_2SO_3 + H_2O$	0.20
$PbO_2 + 4H^+ + SO_4^{2-} + 2e^- \rightarrow PbSO_4 + 2H_2O$	1.69	$Cu^{2+} + e^- \rightarrow Cu^+$	0.16
$MnO_4^- + 4H^+ + 3e^- \rightarrow MnO_2 + 2H_2O$	1.68	$2H^+ + 2e^- \rightarrow H_2$	0.00
$2e^- + 2H^+ + IO_4^- \rightarrow IO_3^- + H_2O$	1.60	$Fe^{3+} + 3e^- \rightarrow Fe$	−0.036
$MnO_4^- + 8H^+ + 5e^- \rightarrow Mn^{2+} + 4H_2O$	1.51	$Pb^{2+} + 2e^- \rightarrow Pb$	−0.13
$Au^{3+} + 3e^- \rightarrow Au$	1.50	$Sn^{2+} + 2e^- \rightarrow Sn$	−0.14
$PbO_2 + 4H^+ + 2e^- \rightarrow Pb^{2+} + 2H_2O$	1.46	$Ni^{2+} + 2e^- \rightarrow Ni$	−0.23
$Cl_2 + 2e^- \rightarrow 2Cl^-$	1.36	$PbSO_4 + 2e^- \rightarrow Pb + SO_4^{2-}$	−0.35
$Cr_2O_7^{2-} + 14H^+ + 6e^- \rightarrow 2Cr^{3+} + 7H_2O$	1.33	$Cd^{2+} + 2e^- \rightarrow Cd$	−0.40
$O_2 + 4H^+ + 4e^- \rightarrow 2H_2O$	1.23	$Fe^{2+} + 2e^- \rightarrow Fe$	−0.44
$MnO_2 + 4H^+ + 2e^- \rightarrow Mn^{2+} + 2H_2O$	1.21	$Cr^{3+} + e^- \rightarrow Cr^{2+}$	−0.50
$IO_3^- + 6H^+ + 5e^- \rightarrow \frac{1}{2}I_2 + 3H_2O$	1.20	$Cr^{3+} + 3e^- \rightarrow Cr$	−0.73
$Br_2 + 2e^- \rightarrow 2Br^-$	1.09	$Zn^{2+} + 2e^- \rightarrow Zn$	−0.76
$VO_2^+ + 2H^+ + e^- \rightarrow VO^{2+} + H_2O$	1.00	$2H_2O + 2e^- \rightarrow H_2 + 2OH^-$	−0.83
$AuCl_4^- + 3e^- \rightarrow Au + 4Cl^-$	0.99	$Mn^{2+} + 2e^- \rightarrow Mn$	−1.18
$NO_3^- + 4H^+ + 3e^- \rightarrow NO + 2H_2O$	0.96	$Al^{3+} + 3e^- \rightarrow Al$	−1.66
$ClO_2 + e^- \rightarrow ClO_2^-$	0.954	$H_2 + 2e^- \rightarrow 2H^-$	−2.23
$2Hg^{2+} + 2e^- \rightarrow Hg_2^{2+}$	0.91	$Mg^{2+} + 2e^- \rightarrow Mg$	−2.37
$Ag^+ + e^- \rightarrow Ag$	0.80	$La^{3+} + 3e^- \rightarrow La$	−2.37
$Hg_2^{2+} + 2e^- \rightarrow 2Hg$	0.80	$Na^+ + e^- \rightarrow Na$	−2.71
$Fe^{3+} + e^- \rightarrow Fe^{2+}$	0.77	$Ca^{2+} + 2e^- \rightarrow Ca$	−2.76
$O_2 + 2H^+ + 2e^- \rightarrow H_2O_2$	0.68	$Ba^{2+} + 2e^- \rightarrow Ba$	−2.90
$MnO_4^- + e^- \rightarrow MnO_4^{2-}$	0.56	$K^+ + e^- \rightarrow K$	−2.92
$I_2 + 2e^- \rightarrow 2I^-$	0.54	$Li^+ + e^- \rightarrow Li$	−3.05
$Cu^+ + e^- \rightarrow Cu$	0.52		

Figure 2.16. Reduction processes and potentials
(Source: René McCormick, 2006)

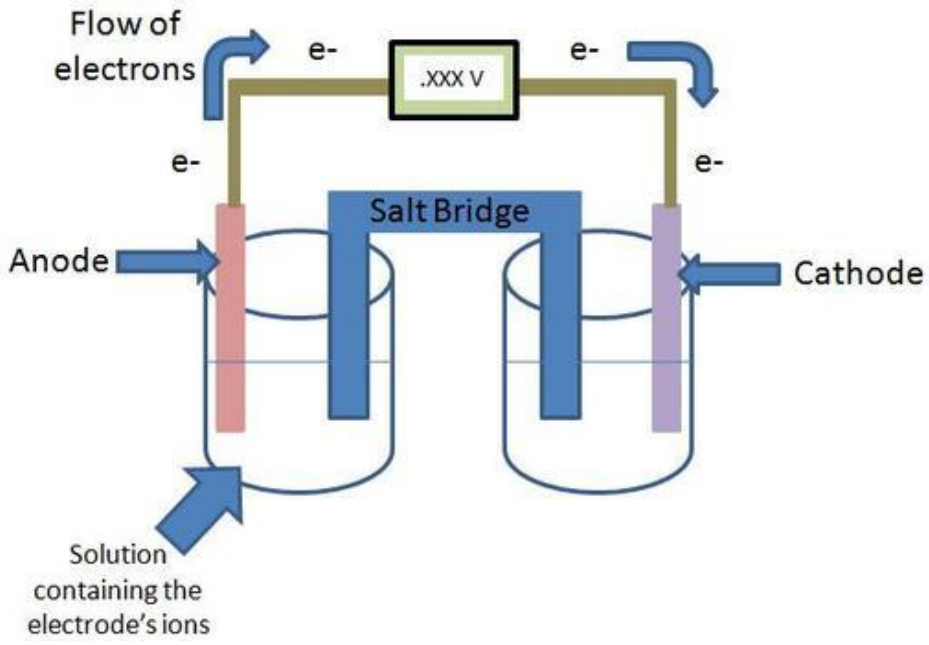

Figure 2.17. An Electrochemical Cell
(Source: Petrucci et al. 2007)

An electrochemical cell is consisted of two electrodes and an ionic conductor called electrolyte (Figure 2.17). Both have charge transfers yet on electrodes it occurs via the motion of electrons, although it occurs via the motion of ions in the electrolyte. At each electrode, an electrochemical reaction occurs. This is named as a half cell reaction. There are two fundamental types of half cell reactions:

- Oxidation reactions
- Reduction reactions

2.5.1. Oxidation-Reduction Reactions

Charge transfers in the electrochemical reactions is defined upon the direction of them. If a molecule accepts the electron, then it is called reduction, if it loses, then it is called oxidation (Figure 2.18).

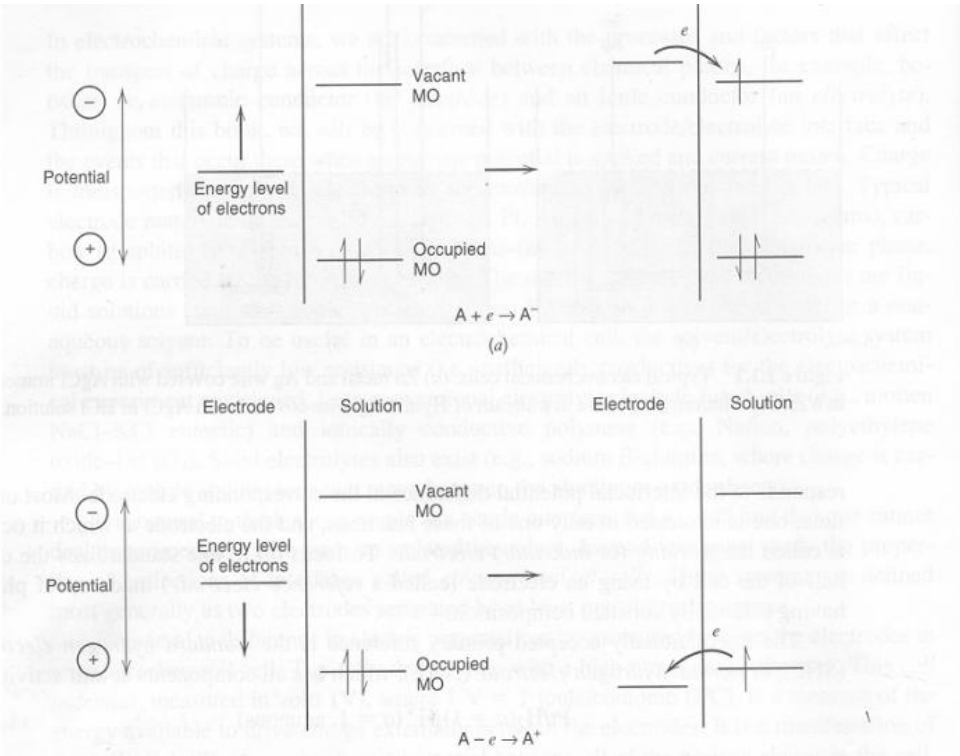

Figure 2.18. Oxidation and Reduction
(Source: Oxidation and Reduction Process, 2015)

This phenomena involves the loss of an electron for oxidation and the transfer of electrons from the metallic structure of the electrode. Moreover it is an energetic process,

and occurs when the energy of the electrode dips below the highest occupied molecular orbital of the molecule. However, reduction involves the gain of an electron and the transfer of electrons from the electrode to the sample. Reduction is also an energetic process, and occurs when the energy of the electrode increases above the lowest vacant orbital of the molecule. The electrodes are used in the oxidation reduction reactions are known as anode and cathode. The electrode where the reaction of attract occurs is called the working electrode and at which the other (coupled) reaction occurs is called the counter electrode. A third electrode, called the reference electrode may also be used. For a given set of two reversible redox reactions, Thermodynamics tells that reaction proceeds as an oxidation and which proceeds as a reduction (Johanna Löberg, Jenny Perez Holmberg, Ingela Mattisson Anna Arvidsson, and Elisabet Ahlberg). The electrode's potential for a reaction is derived directly from the free energy difference for that reaction $\Delta G = -nFE$ where G is used for Gibbs free energy, n is used here as number of Faradays passing through the cell, F is for Faraday constant and E is the electromotive force of the cell. By this method, for instance, the reaction with the lower standard reduction potential gets oxidized, the other reaction maintains as a reduction.

$Zn \leftrightharpoons Zn_2^+ + 2e$, $E°_{red} = 0.7618$ V

$Cu_2^+ + 2e \leftrightharpoons Cu$, $E°_{red} = 0.341$ V

Thus, in the example above, Zn is oxidized, and Cu is reduced which can also be understood from direction of the 2e. As a result

$$E_{cell} = E_{cathode} - E_{anode} \tag{2.1}$$

Since E cell must be positive, E cathode must be bigger than E anode.

As a matter of fact that,

$$m = \frac{M \,.\, I \,.\, t}{n \,.\, F \,.\, m} \tag{2.2}$$

m - mass of substance

M - molecular weight of the substance

I - current passed

t - time for which the current is passed

n - number of electrons transferred

F - Faraday constant (96475 C / eqv)

So the amount of substance is directly proportional to the density of the current passed.

There are two main types of methods which can easily use electrochemical charecterizations and analyse of the measurements those are called Cyclic Voltammetry and Lineer Sweep Voltammetry. Due to its nano-amount quantities, Cyclic Voltammetry had been chosen and measurements were done on sticks in Faraday Cage with Palme Sense.

2.5.2. Cyclic Voltammetry

Today linear potential scan methods are very practical tools for initial studies of new systems and proved to be reliable techniques to get information about totally complicated electrode reactions. Cyclic voltammetric methods, in particular, have often been benefited in basic studies of electrochemical systems and in the concept of analytical research.A cyclic voltammetry is potentiodynamic electrochemical instrument which can be tried on the sample when electrical potential is increased and shrinked by time linearly. An initial potential is applied on the sample(working electrode) and it is scaled up to set point to observe changes due to potential and then is scaled down to the initial point but this time reverse direction which is set by the user initially in terms of potential and current (Figure 2.19).

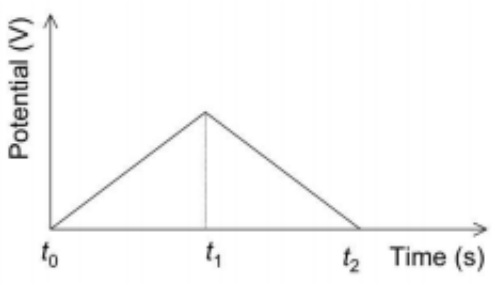

Figure 2.19 Applied Potential in Cylic Voltammetry
(Source: Nicholson, R. S., 1964)

The graph which is created and presented by CV instrument is called a voltammogram. It gives a graph which has a behaviour of the working elecrode's response owing to the variable applied voltages (Figure 2.20). An ideal voltammogram should be like that at least with two runs and the applied potential versus current peaks would be used for oxidation and reduction parts to measure band-gaps density lately (P.He, L.R. Faulkner, Anal.Chem). The red graph represents the second run of the characterization which must be the same or very similar to the old one. Voltammetric measurements are carried out with the help of using an electrochemical cell made up of three electrodes immersed in a solution containing the combination of chemical salts and deionized water which must be nonreactive. One of the three electrodes is the working electrode, which is typically made of platinum, gold, silver, glassy carbon, nickel, or palladium. The redox process occurs upon this electrode. Its dimensions are held very small in order to enhance its tendency to become polarized. The second electrode is generally known as reference electrode, which provides calibration for the applied potential. Examples of commonly used reference electrodes are the normal hydrogen electrode, Ag/AgCl electrode, and calomel electrode (i.e., Hg/Hg_2Cl_2). The third electrode is called the counter electrode, which is often a platinum wire that simply serves to conduct electricity from the current source through the liquid conductor solution to the other two electrodes.

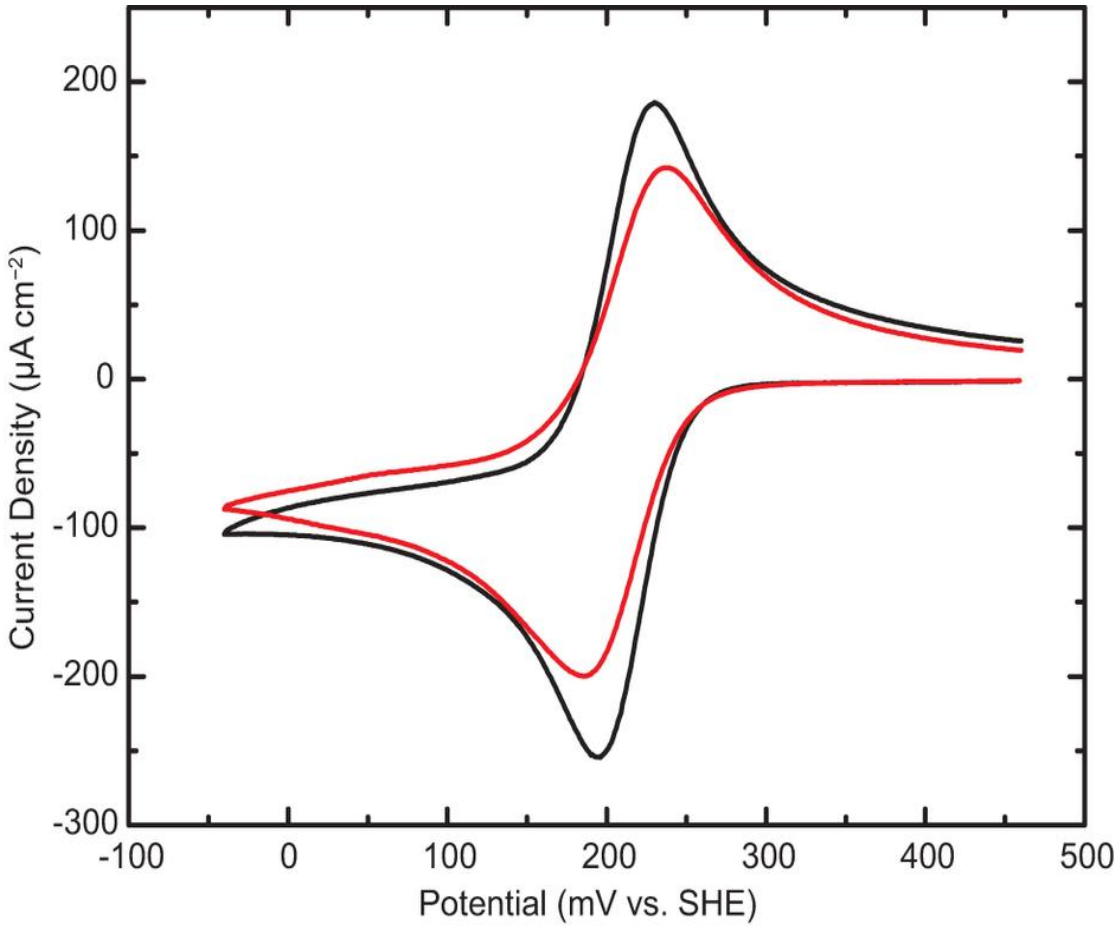

Figure 2.20. An Ideal Voltammogram
(Source: Huskinson B et al. 2014)

These two graphs red and black refer to the duplicated runs with CV which is essential for repeatability testing.The redox potential can be obtained from a voltammogram by calculating the average value of the anodic and cathodic peaks. For example, for the voltammogram shown in (Equation 2.3), the one-electron ($E_{1,\,1/2}$) and two-electron ($E_{2,1/2}$) redox potentials can be calculated as:

$$E_{1,1/2} = \frac{E_1^c + E_1^a}{2} \text{ and } E_{2,1/2} = \frac{E_2^c + E_2^a}{2} \qquad (2.3)$$

The subscript 1/2 indicates that the potential is obtained approximately at the half-height of the cathodic and anodic peaks and hence is often called the half-wave potential. At these points the concentrations of the reduced and oxidized molecules have to be equal.

In a typical voltammogram, both thermodynamic and kinetic information are available in a single experiment.

The experimenter can understand details about the rates of electron transfer, as shown in Figure 2.21, between substances and electrodes and one can also learn about the rates and nature of chemical processes coupled to the electron transfer event during the process. The properties of both reactants and products can frequently be discerned from a single voltammogram, or from a series of voltammograms obtained as a function of scan rate, molar density, pH, solvent type, and fabrication temperature .

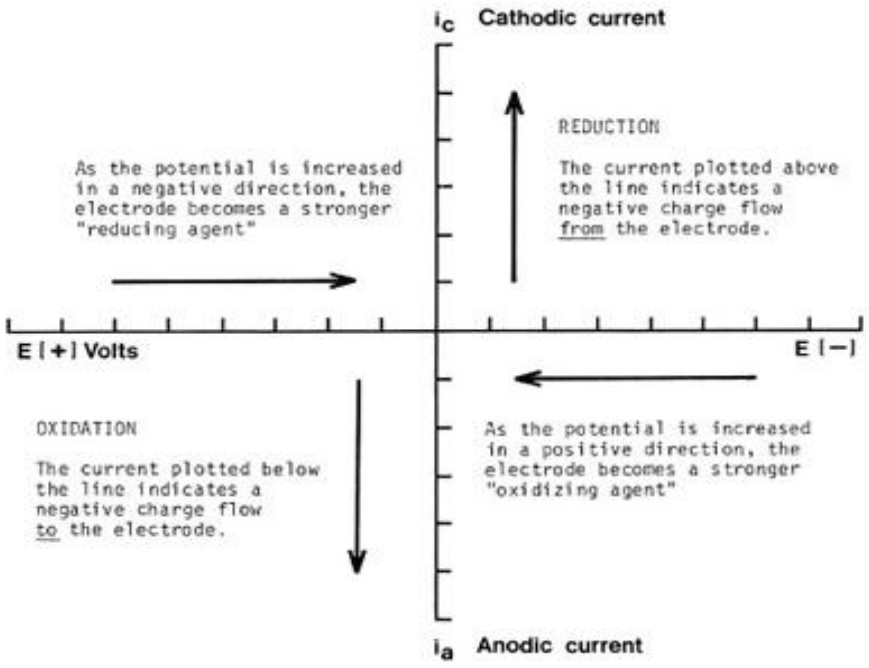

Figure 2.21 Electrochemical interactions of a typical voltammogram onto regional base. (Source: Cyclic Voltammetry, 2015)

The speed of change on potential is arranged with the scan rate function due to the fact that some radicals could only be prevented before they influence redox reactions. (DuVall, Stacy DuVall; McCreery, Richard, 1999).

The potential applied, E, will control the concentration of the two redox forms in accordance with the Nernst equation:

$$E = E_0 + (\frac{RT}{nF})\, ln\, \frac{[Ox]}{[Red]} \qquad (2.4)$$

Where, Ox = oxidised species

Red = reduced species

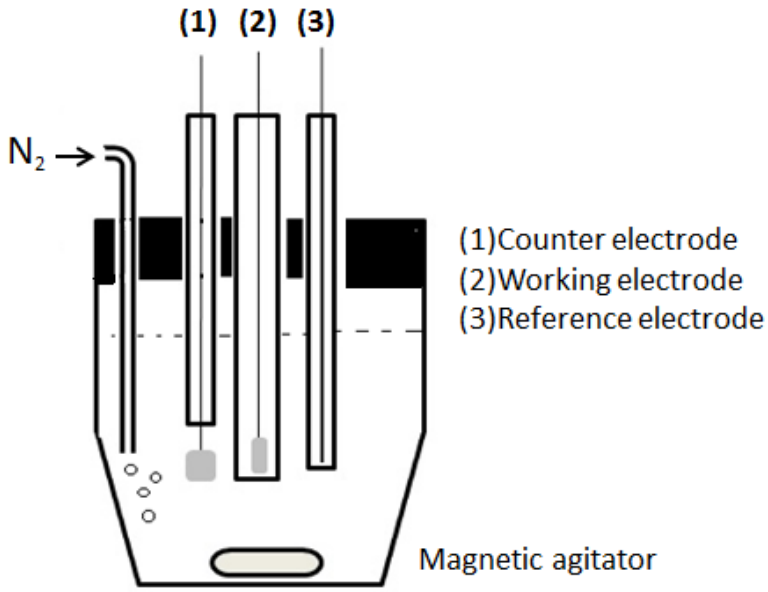

Figure 2.22. The schematic illustration of the CV system fundementally, is working with electrolyte solution as expected. (Source: Cardoso et al. 2014)

The application of CV as a dynamic measuring technique is based on the assumption of a linear rise and fall of the potentialversus current (Figure 2.22). In order to guarantee successful analysis, the electrochemical workstation has to treat the scan function with high accuracy and must avoid interruptions, especially for caused by autoranging functions. Therefore CV is performed in a fixed current measurement range, defined by the user through the limiting current input. It is important to select an appropriate current range, which is warned with the instrument as low current, to avoid restarting on current overdrive with shrinked voltage scale on the one hand and an accurate signal-tonoise ratio on the other hand. In the literature, there are few examples showing the capability of CV on various examples. For instance Figure 2.23, voltammograms show lots of peaks for the samples ZnO and P25 (TiO_2) in KCl solutions with or without Methylne Blue in the scale of current versus potential.

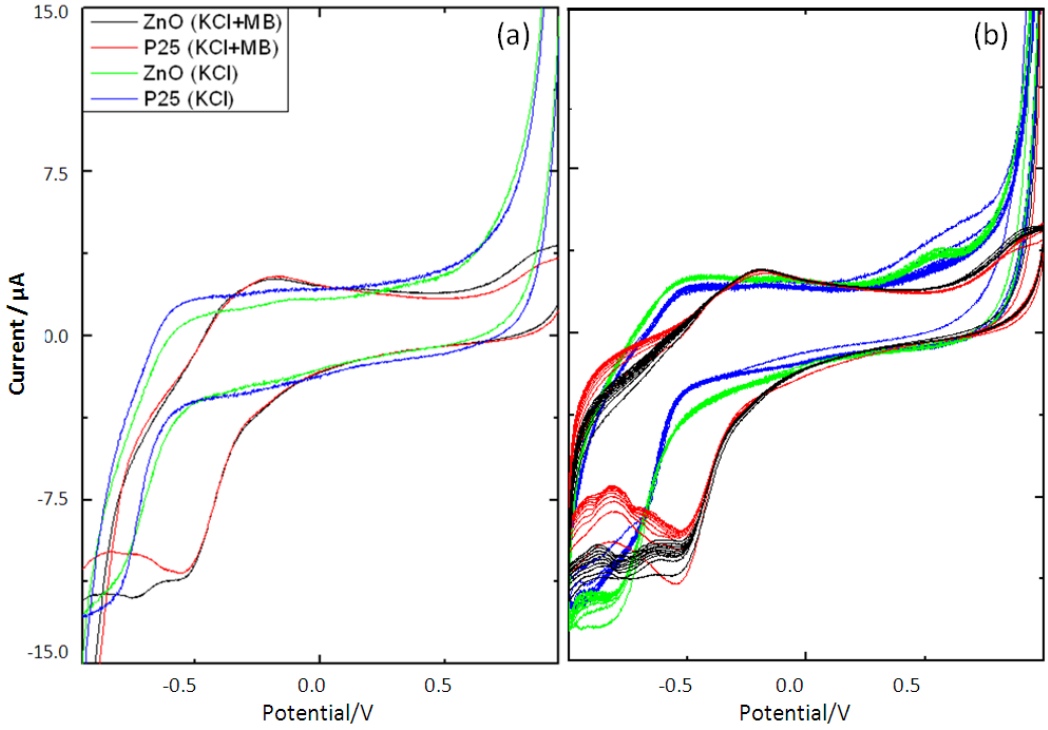

Figure 2.23. The schematic illustration of a typical CV (a) CV and (b) multiple CV of modified GCE in 0.1 M of KCl solution, MB is methylane blue. (Source: Fatin S O et al. 2012)

Differences can easily be detected by this kind of analysis such as in graph (a) P25 could not obtain peaks even though MB added P25 could get definite peaks shown in the red voltammogram.

Another voltammogram is examined in Figure 2.24. At those graphs, before and after conditions are compared by the help of Cyclic Voltammetry in a photoreaction medium. As seen, after a photoreaction, because of the new reductive species, peak was appeared at −0.36V (versus SCE), and it probably was due to the nonstoichiometric intermediate of CoO*x* active species which was produced during photoreaction process.

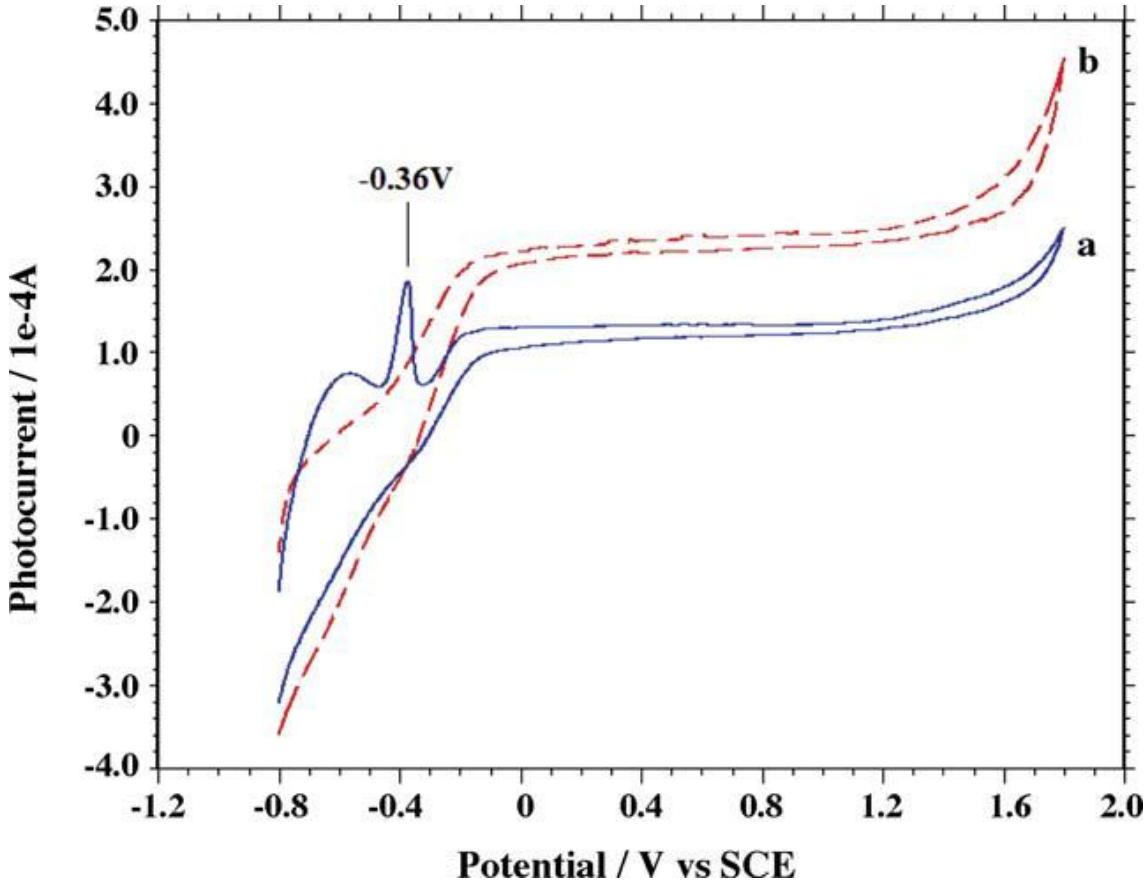

Figure 2.24. The existance or non existance of cyclic voltammograms and peaks (a) After photoreaction and (b) before photoreaction for 0.4 wt% $CoOxTiO_2$ electrodes before and after photoreaction with illumination Solution: 0.1 mol Na_2SO_4, Scan rate, $50mVs^{-1}$. (Source: Wu Y. et al. 2006)

In Figure 2.25, CV is performed for both pure and iodine doped TiO_2 samples. The working electrode was polarized from the rest potential in the anodic direction up to 1 V and back up to -1 V vs. Ag/AgCl reference electrode within 0.1M KCl. In general, the shape of CV curve is typical for titanium dioxide materials with a marginal capacitive current in anodic region (seen with A). However, in the case of doped materials, the clear reduction peak marked as B at 0.2 V vs. Ag/AgCl reference electrode again 0.1M KCl is that is why presence of dopant atoms. This cathodic peak can be described as the reduction of Ti^{4+} sites in TiO_2. As a result of the electrochemical reaction, the change in the electronic structure of TiO_2 takes place. This change is the formation of additional energy levels within the bandgap directly influences the conductivity parameters causing different current densities.

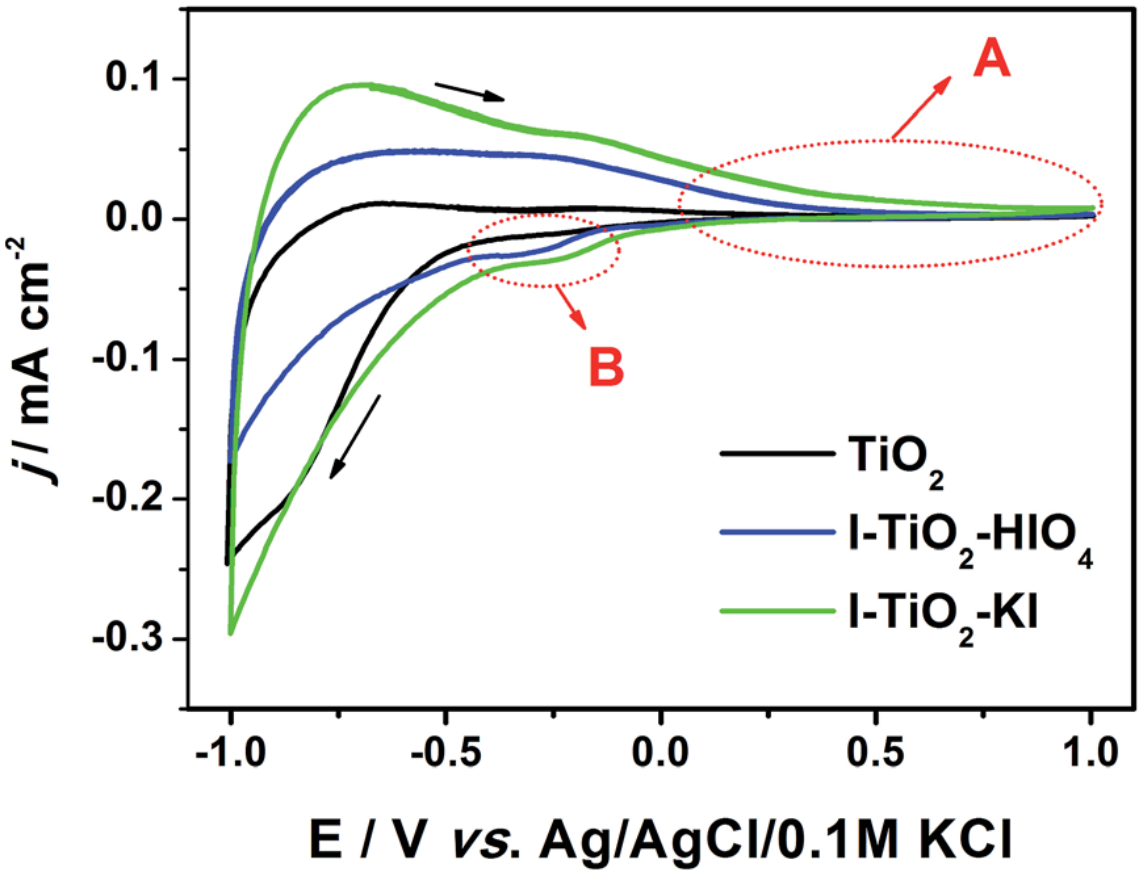

Figure 2.25. Cyclic voltammetry curves recorded for doped and pristine TiO_2, immersed in 0.1 M K_2SO_4, at a scan rate 50 mV/s (Source: Siuzdak et al. 2015)

Measuring voltage versus current be used for comparison between the Capacitance Values of different samples within the voltammograms. In Figure 2.26, 7 different samples were applied which were respectiveley named as sample 1,2,3,..etc. Sample forms of the TiO_2 were shown in table 2.2 . Their specific capacitances were used the equation below :

$$C = Q/ (m \times \Delta V). \quad (2.5)$$

where C is the specific capacitance calculated based on the mass of active material, Q is the charge calculated using half the integral area of the CV curve, m is the mass (g) of the active material, and ΔV is the potential difference. The C values of the samples are summarized in Table 2.2.

Table 2.2 Sample structures and calculated specific capacitances

Samples	Specific capacitance (mF g^{-1})	BET areas[a] ($m^2 g^{-1}$)	Featured structure[b]
Sample 1	1729	68.5	TiO_2 nanodishes
Sample 2	460	47.1	TiO_2 three-layer nanosheets
Sample 3	1361	51.6	TiO_2 ancient Chinese coins
Sample 4	270	12.6	TiO_2 single-layer nanosheets
Sample 5	1493	4.6	$TiOF_2$ nanocubes
Sample 6	365	0.9	Hollow TiO_2 nanocubes
Sample 7	1193	50.0	Commercial rutile TiO_2

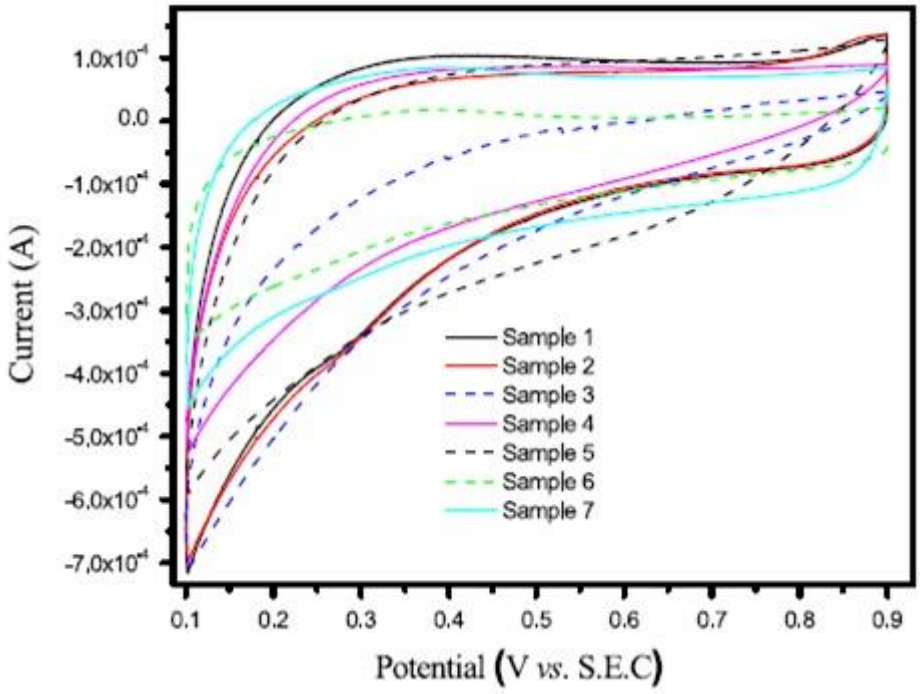

Figure 2.26. Cyclic voltammetry curves for variously prepared TiO_2 samples. (Source: Sunqi Lou et al. 2015)

Polyaniline/graphene/titania nanotube arrays (PGTNs) and Polyaniline/titania nanotube arrays (PTNs) were tried in CV for a kind of electrochemical analyses also scan rate differencies were observed in Figure 2.27.

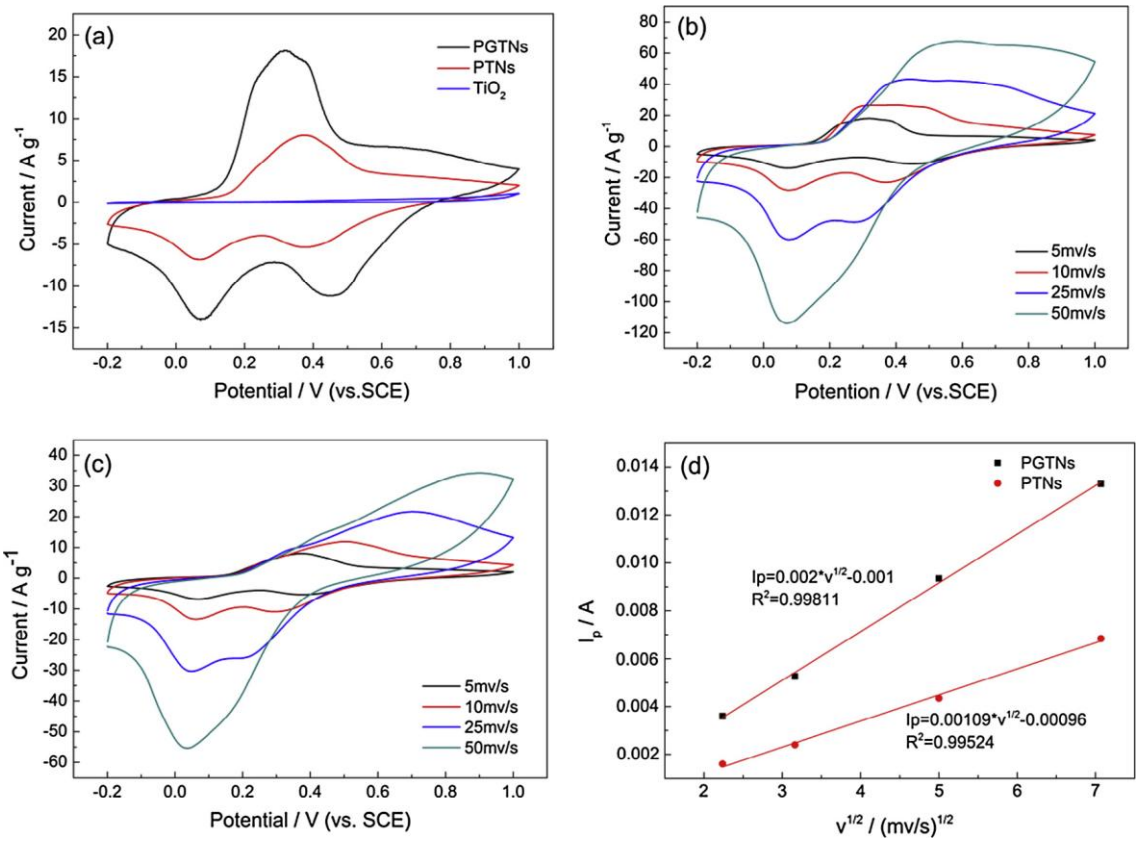

Figure 2.27. (a) Voltammograms of PGTNs, PTNs and TiO_2 at 5 mV. (b–c) CV curves of PGTNs and PTNs at different scan rates. (d) Square roots of various scan rates (v1/2) vs. Oxidation peak current (Ip). (Source: Hua Huang et al, 2015)

CHAPTER 3

EXPERIMENTAL

3.1. Preparation of the Films

Rare Earth Element (REE) doped TiO_2 powders were prepared by sol-gel using titanium tetraisopropoxide (TTIP, Aldrich 97%) as titanium precursor. Cerium(III) nitrate hexahydrate ($Ce(NO_3)_3.6H_2O$, Aldrich 99.99% trace metal basis), neodymium nitrate hexahdrate ($Nd(NO_3)_3.6H_2O$, Aldrich 99.99% trace metal basis), lanthanum nitrate hexahydrate ($La(NO_3)_3.6H_2O$, Aldrich 99.99% trace metal basis), erbium(III) nitrate pentahydrate ($Er(NO_3)_3.5H_2O$, Aldrich 99.9% trace metal basis), were used as dopant precursors.

Pure TiO_2 powder was prepared by the dropwise addition of a solution (nitric acid (HNO_3, Merck 65%) and water in ethanol (Merck absolute) to a titanium tetraisopropoxide/ethanol solution under vigorous stirring at room temperature. The resulting transparent sol with the molar ratios of TTIP:H_2O:HNO_3:EtOH as 1:2:0.06:5.9 was stirred until complete gelation was observed. REE doped TiO_2 powders were prepared by following the same route with the addition of predetermined amounts of RE nitrates to nitric acid/water/ethanol solution. The obtained gels were dried at 50^oC overnight prior to heat treatment at 700^oC for 3 hours. TiO_2 powders doped with 0-20% RE_2O_3 ,Rare Earth Oxide, (on molar basis) were prepared in the context of this study. A schematic representation for the preparation of REE doped sol-gel TiO_2 powders is given in Figure 3.1.

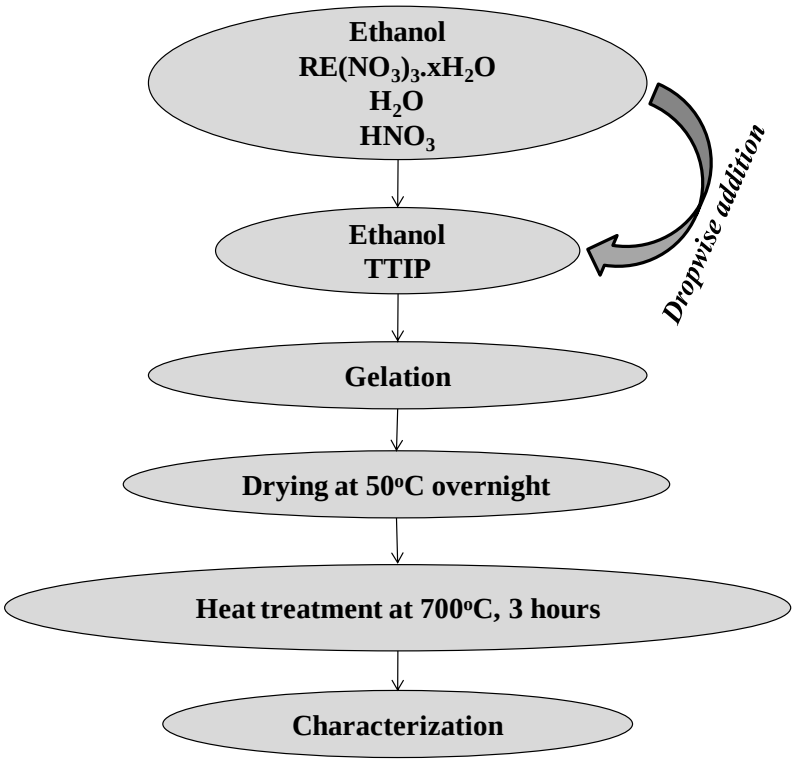

Figure 3.1. A schematic representation of REE doped sol-gel TiO_2 powder preparation process.

TiO_2 film coated ITO (Indium Tin Oxide) glasses were prepared by using doctor-blade technique. Doctor blade (or tape casting) is one of the widely used methods for producing techniques and it is accepted as precision accurate coating method. When a constant relative movement is established between the blade and the substrate, the slurry spreads on the substrate to form a teen layer which results in a gel layer to dry. So, first, TiO_2 pastes were prepared with PEG200/water with different pure/doped TiO_2 powders. The pastes were applied on the ITO glasses by using doctor-blade technique. Then the films were dried at room temperature and heat treated at 400^oC for 2 hours for burning off organics and adhesion of the TiO_2 films on ITO glasses. Prepared films are shown in Figures 3.2 and 3.3.

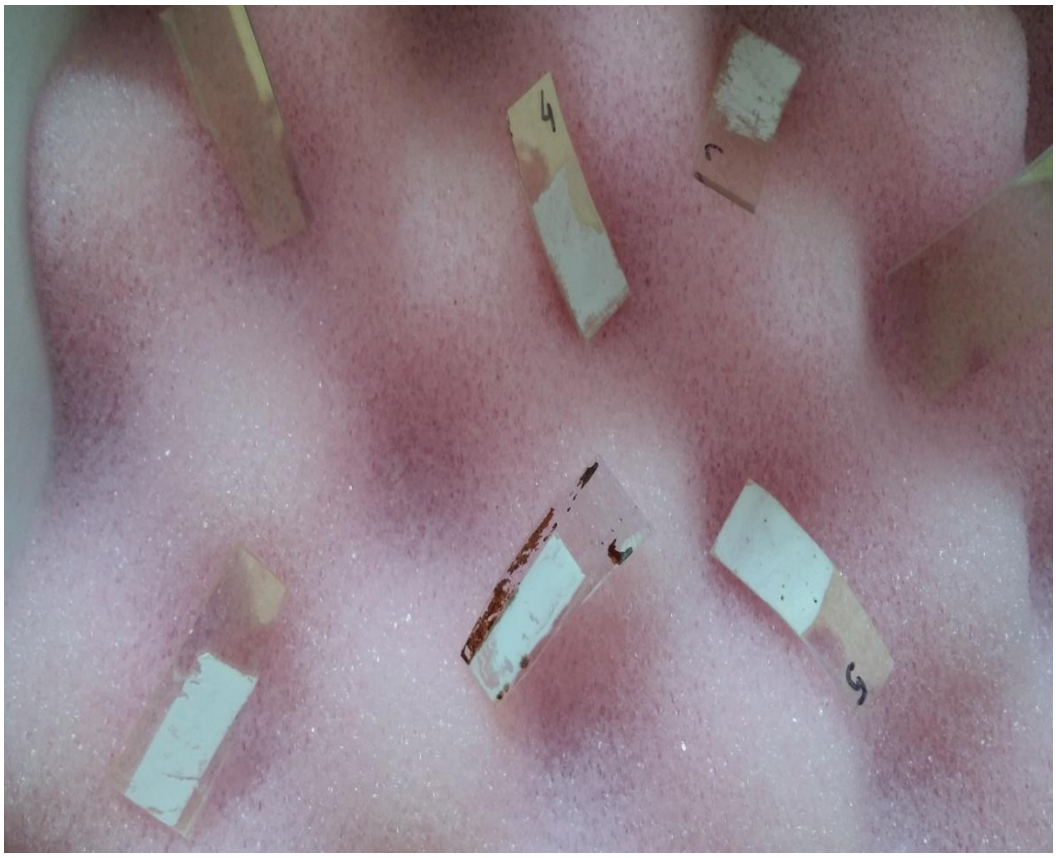

Figure 3.2. TiO_2 film coated ITO glasses prepared by doctor-blade technique.

Figure 3.3.Colour Change of Titania Powders

Titanium sticks were used due to difficulties in the application of large ITO glasses in CV measurements and low adhesion of the powders on the glasses. Sticks were coated with doped/pure TiO_2 by using the corresponding sols of the previously prepared powders. Pure/doped TiO_2 sols were prepared with ¼ of Ti^{4+} concentration of the powder recipes, whereas H_2O/Ti^{4+} and H_3O^+/Ti^{4+} ratios were kept constant. Image of cerium doped TiO_2 sol is given in Figure 3.4.

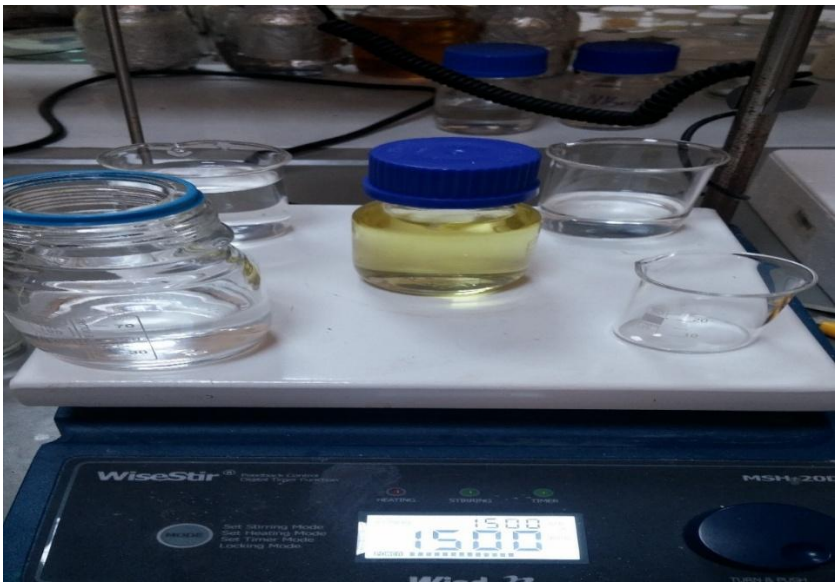

Figure 3.4. Image of cerium doped TiO_2 sol.

Pure/doped TiO_2 coated titanium sticks were prepared by using dip-coating method. Following procedure was employed:

1- 1 m of titanium stick/bar with 2 mm diameter was cut into 7.5 cm pieces.
2- Titanium pieces were cleaned with ethanol and dried.
3- Sticks were dipped into TiO_2 sols and waited for 30 seconds.
4- Step 3 was repeated for 5 times for obtaining thick TiO_2 films.
5- Coated sticks were dried at room temperature for 1 hour (Figure 3.5).
7- Dried sticks were heat treated at 700^oC for 3 hours (Figure 3.6).

Figure 3.5. Drying the Sticks

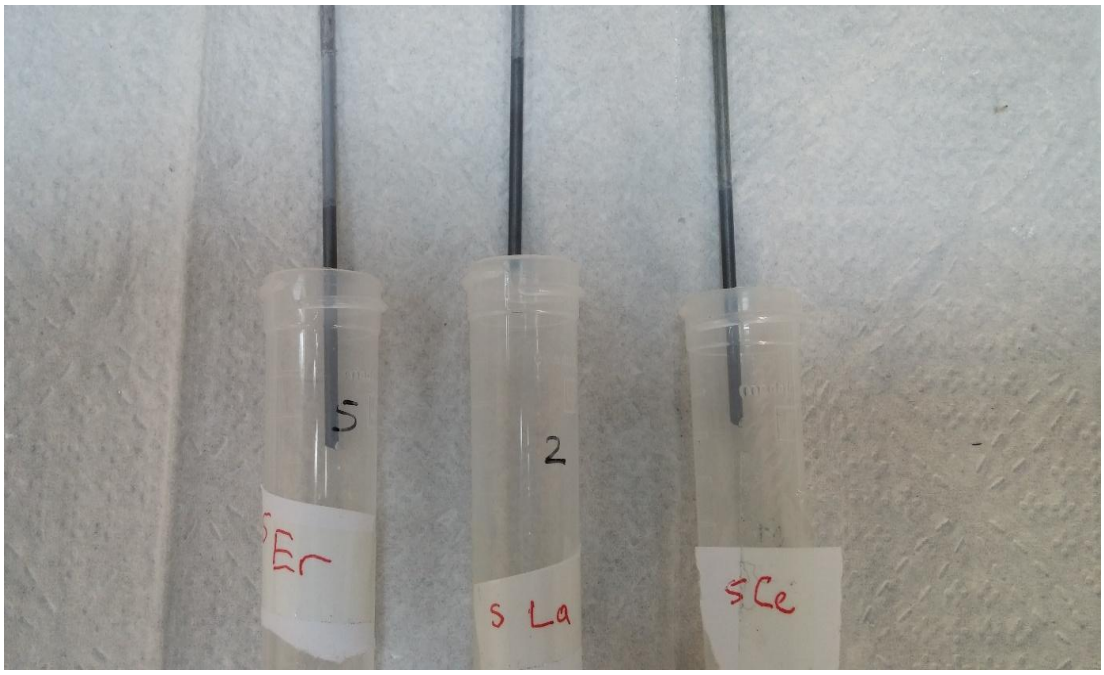

Figure 3.6. TiO_2 coated titanium sticks.

3.2. Characterization of the Films

Phase characterization of the prepared powders was performed by Philips X'pert Pro XRD equipment with monochromated high-intensity (λ=1.54Å) CuKα radiation. The scanning rate was set as 2.5 2Θ/min between 5^o and 80^o with 0.033^o step size. Characterization was conducted with 1-2 g powder pressed in an aluminum cassette which was also used as reference material to calculate the accurate peak positions.

Dynamic light scattering (DLS) analyses were conducted with Malvern Zetasizer 3000HS DLS in order to determine doped/undoped TiO_2 sol average particle sizes.

Scanning electron microscopy (SEM) analysis were conducted with FEI QUANTA 250 FEG.

3.3. CV Measurements

Cyclic voltammetry measurements were conducted in a three-electrode undivided glass cell (Palm Sense). The experimental setup for CV measurements consists of CV instrument, three-electrode glass cell in a faraday cage and a computer The images of the three-electrode undivided glass cell and experimental setup used in CV measurement are given in Figures 3.7 and 3.8, respectively.

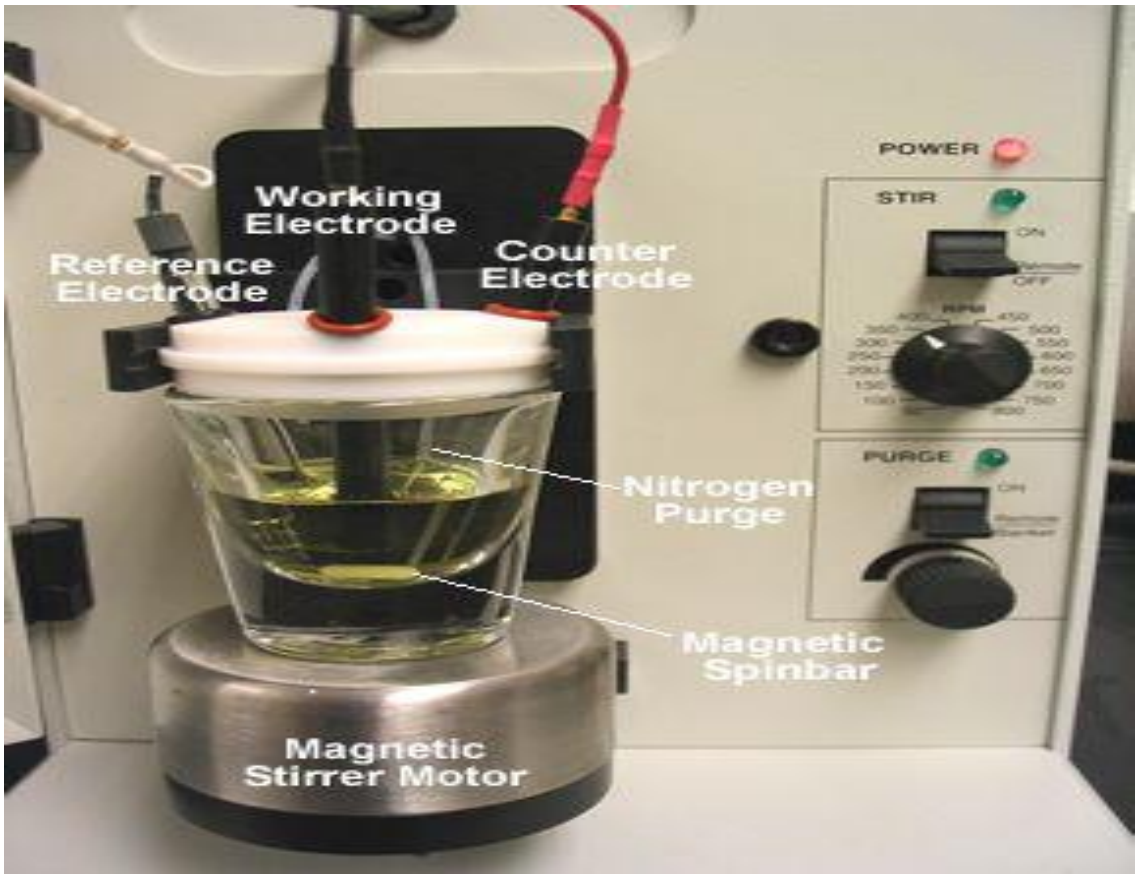

Figure 3.7. Three-electrode cell for CV measurements.

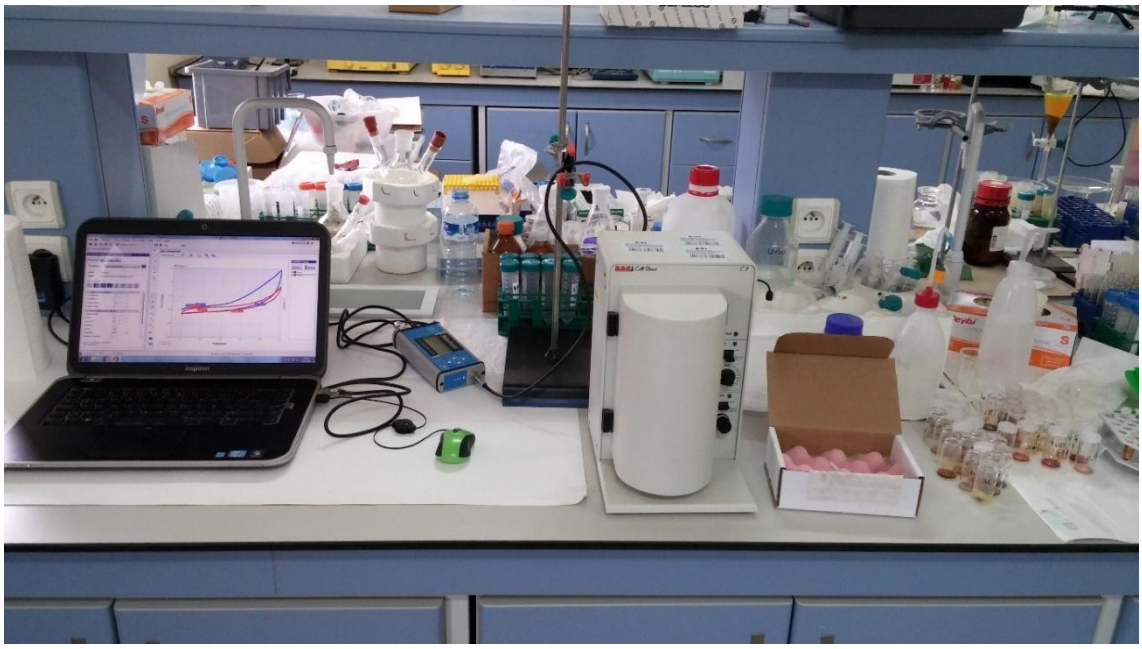

Figure 3.8. Experimental setup for CV measurements.

The electrolyte solutions were 0.1 M KCl or 0.1 M NaOH solution purged with CO_2 (g) for 30 min. The second solution was used since photocatalytic reduction of CO_2 was generally conducted in this solution in the studies on artificial photosynthesis. The solution was purged with N_2 before the CV mesurements when KCl solution was used as shown in Figure 3.9.

Figure 3.9. N_2 purging of 0.1 M KCl solution.

The experimental conditions such as supporting material (ITO glass or titanium stick), electrolyte, potential range, scan rate employed for different pure/doped TiO_2 films and the determined oxidation/reduction points is given in Table 4.1

CHAPTER 4

RESULTS AND DISCUSSION

4.1. Characterization of the Powders and Sols

XRD patterns of pure/doped TiO_2 powders heat treated at 700°C are given in Figure 4.1. It was found that anatase coexists with the rutile phase at 700°C with a contribution of 30.4 wt% for pure TiO2. The relative intensity of (101) reflection peak significantly decreased and FWHM of this peak increased with increasing doping level which indicated that anatase to rutile phase transformation was significantly inhibited by REE doping. The level of this inhibition was found to increase with increasing dopant concentration. The REE doped titania mainly consists of the anatase phase at this heat treatment temperature.

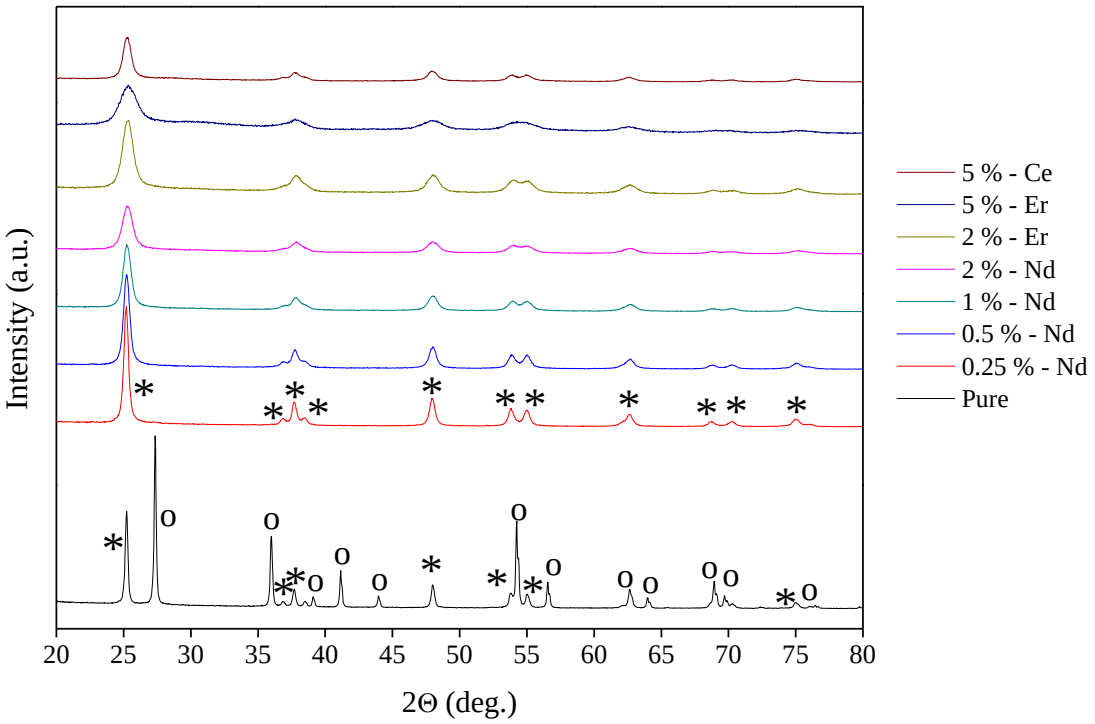

Figure 4.1. XRD patterns of the prepared powders (* and o indicate anatase and rutile phase peaks respectively).

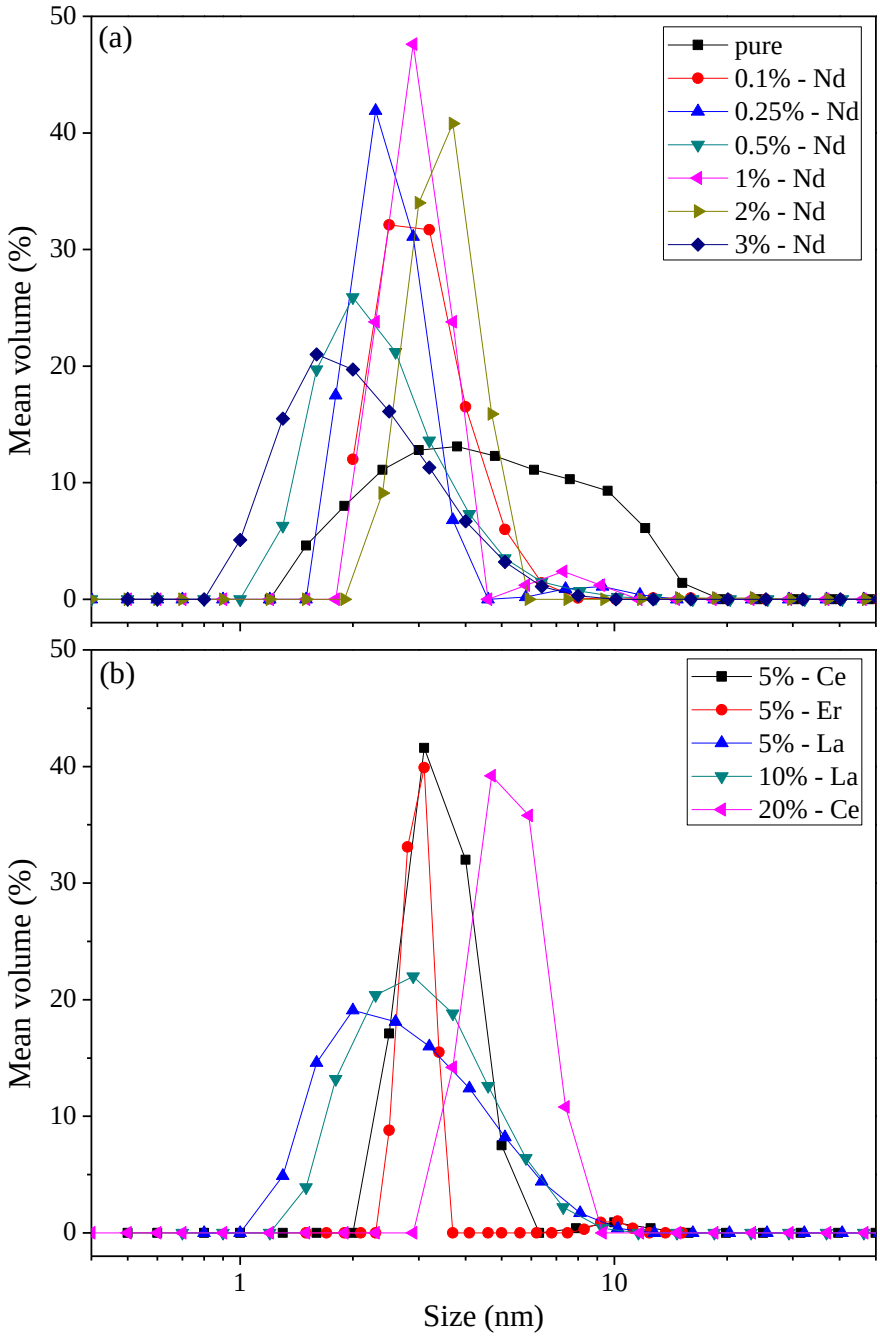

Figure 4.2. Size distributions of the prepared sols.

The sol particle size distributions given in Figure 4.2a and 4.2b indicate the presence of polymeric titania species with sizes in the 1-10 nm range as they are prepared at room temperature. The polymeric sol particles become smaller at low dopant concentrations compared to the pure titania. The presence of such small particles was determined to cause the formation relatively small (~10-20 nm) crystallites in the heat treated powders. The dopant presence even at very low concentrations significantly

reduced the crystallite sizes in the powders as determined from the XRD patterns by Schrerer equation.

4.2. Characterization of the Films

The surface morphologies of the uncoated metallic support stick was investigated by analysing optic microscope images. An example of these optical microscope images is given in Figure 4.3. Although due to the relatively large diameter of the wire the picture is partially out of focus, a clean metallic surface with large scratches due to mechanical polishing was detected. The surfaces were free from any debri or titania films prior to the coating proces.

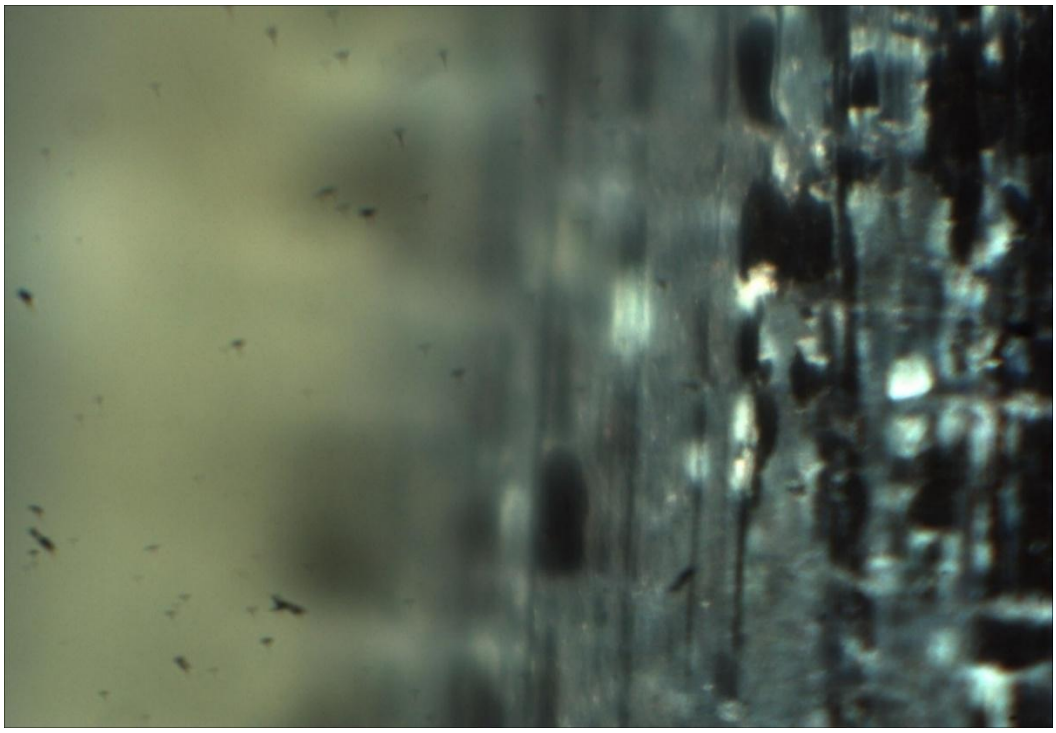

Figure 4.3. Bare titanium stick.

The presence of colourful islands under the microscope was observed to indicate the presene of a thin oxide surface coating on the metallic support wire. These supports were used several times after the film removal by using sand paper and ultrasonic cleaning of the metallic surfaces. The optical microscope photograph of one of the coted surfaces given in Figure 4.4 indicated the presence of a cracked top surface of the films. These

cracks are expected during the relatively fast solvent removal stage of the film formation and subsequent densification/shrinkage occurring in the films. As a result of this observation the film formation process was repeated 4-5 times after the drying of each layer in order to obtain a continous film on the metallic surface with no exposure of the mellic surface to the electrolyte during the successive Cylic voltammetry experiments.

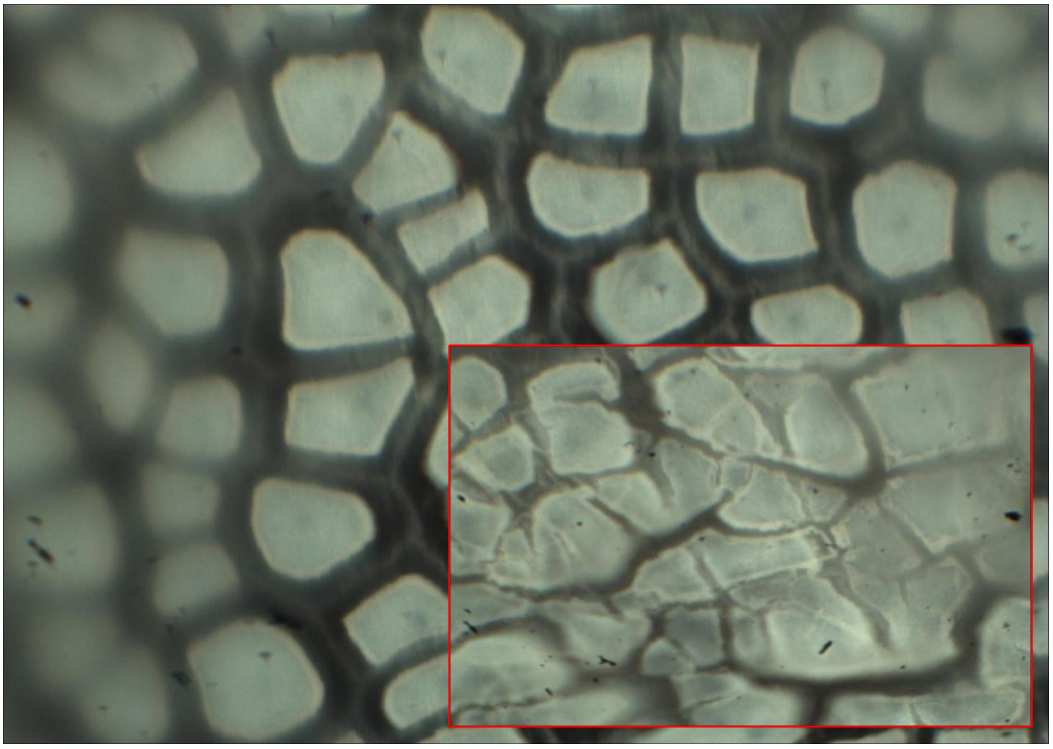

Figure 4.4. Ce doped TiO2 coated titanium stick.

The SEM micrographs of the uncoated and coated titanium wires are presented in Figures 4.5 and 4.6 respectively. The bare metallic surface has almost no features other than some pits resulting from metallic forming and mechanical polishing. The presence of titania coating on the metallic surface is clearly visible in the four micrographs (100X, 1kX,5 kX and 10 kX similar magnifications with uncoted metallic surface SEM's). The presence of an almost coherent film can be seen especially in the 1 kX micrograph. There are relatively large cracked film pieces about 10 microns in thickness on the films. This cracked nature of the top layers partially can be due to the sample preparation for the SEM analysis.

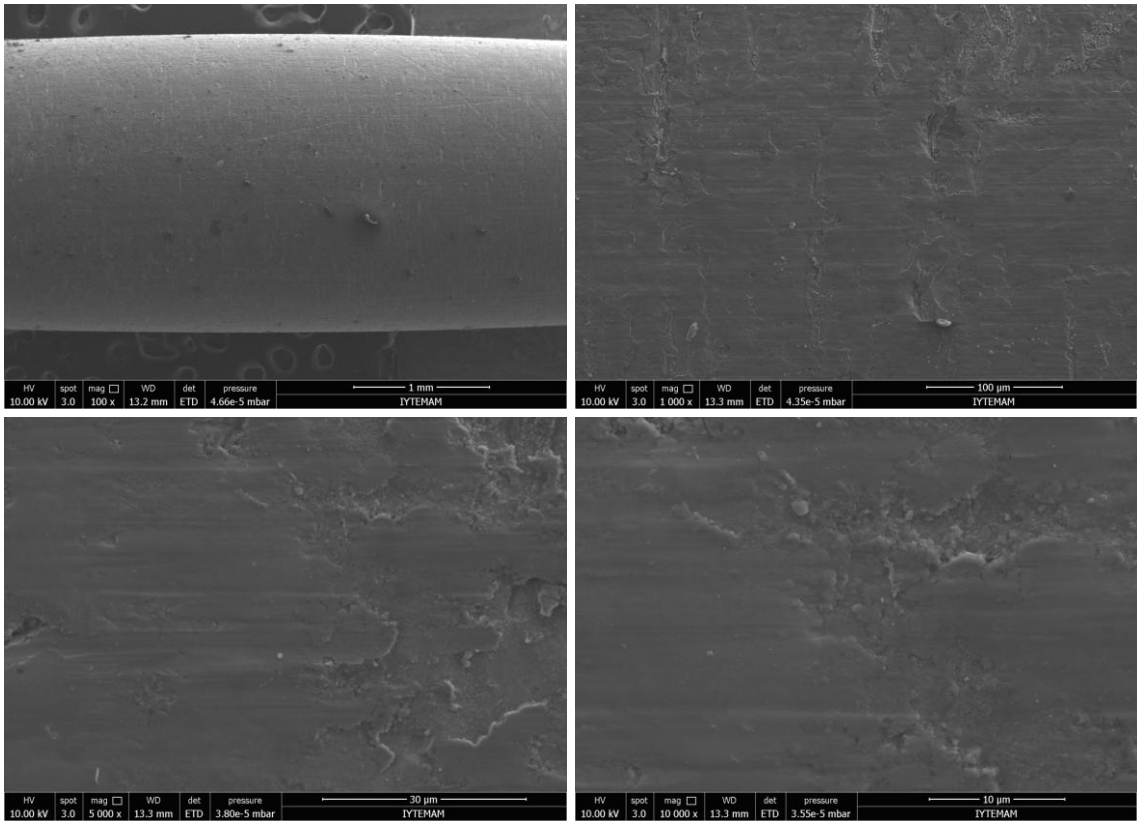

Figure 4.5. SEM images of the bare titanium sticks.

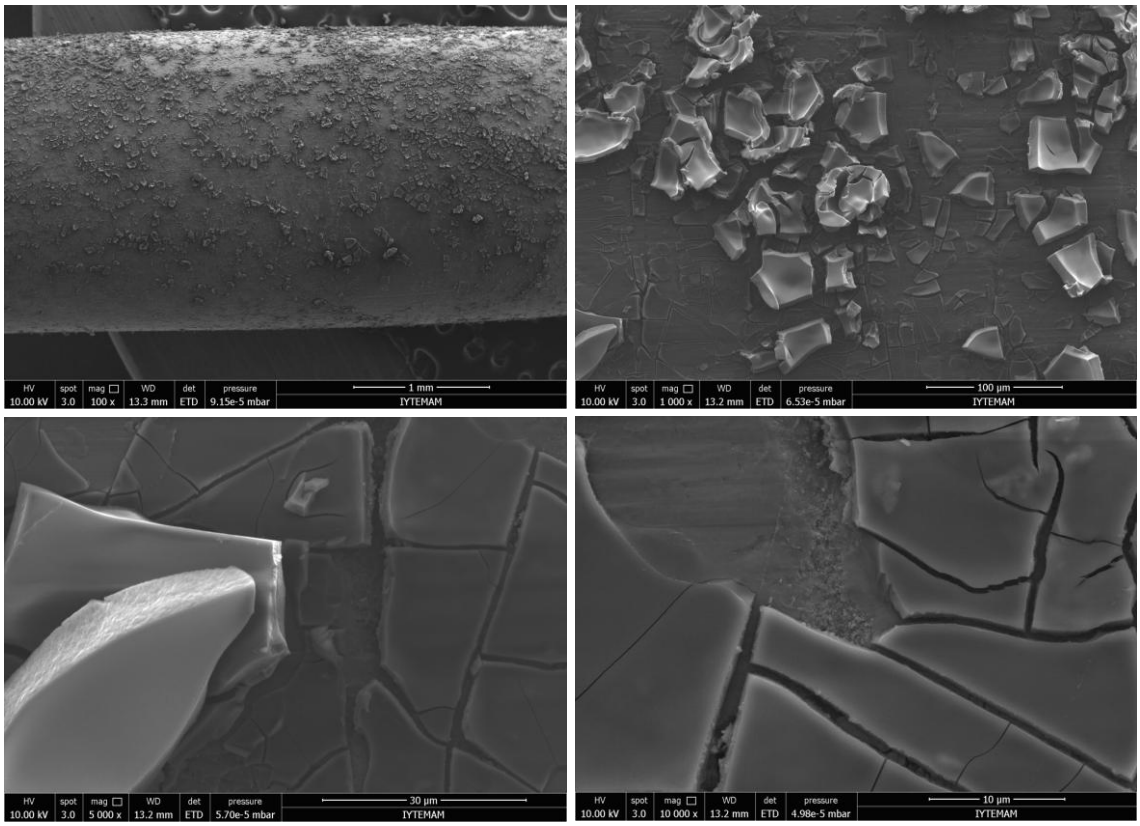

Figure 4.6. SEM images of Nb doped TiO_2 film coated titanium sticks.

4.3. CV Measurements

Titanium electrodes have been used since 1950s for electrochemical reactions (By P. C. S. Hayfield Bickenhill. West Midlands. England. 1998). ITO glasses are also used in various experiments about photocatalyses. Transparency, for this kind of a reaction gains a huge popularity (Daniel G.Nocera. 2011). However, the color change of the titania coated glasses, made titanium sticks useful. Thus, the method was formed on the Titanium wires generally and all parameters of electrochemical measurements have ever been employed can be found in Table 4.1 for both ITO and titanium wire electrodes.

Table 4.1. Experimental conditions.

Sample	Scan rate	Potential range	Doping amount	Electrolyte	Purged gas
Bare ITO Bare titanium stick Nd doped Er doped Ce doped La doped	100mV/s 400mV/s 500mV/s 600mV/s 700mV/s 800mV/s 900mV/s	-1.8. 1.8 (v) -1.8. 1.2 (v) -1.8. 0 (v) -1.8. -0.5 (v) -1.2. 1.2 (v) -1.6. -1.6 (v)	0.1 % 0.25 % 0.5 % 1 % 4 % 5 % 10 %	NaOH KCl KOH $LiClO_4$ $NaClO_4$	CO_2 N_2

These parameters were totally tried, results were compared in a this section below.

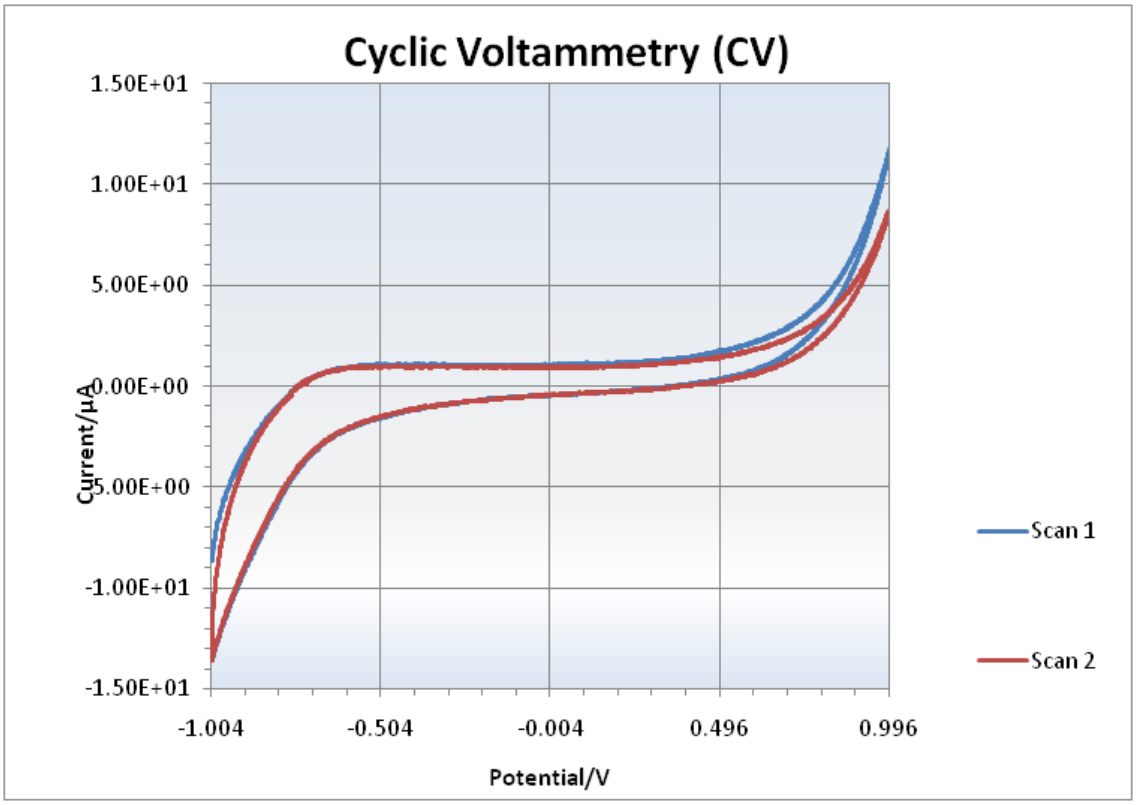

Figure 4.7. CV voltagram of bare titanium stick.

The cyclic voltammetry curves were recorded in Figure 4.7 for pristine titanium wire which was immersed into KCl aqueous solution (N purged). A potential difference was applied between 1V and -1V. There would not be any redox reaction.

Because of the usage of bare sample, oxidation and reduction reactions haven't expected. As expected, a stable behaviour contiuned at the middles and shrinked at about -0.7 V. The net increase started at the positive side at nearly 0.7 V before reverse potential applied. This type of a graph is named as "clean" due to its simple configuration. For instance, titanium stick could be interacted with the O_2 molecules made TiO_2 compound which may form redox reactions. Moreover other dusts may contribute and cause the lack of control within the analyses.

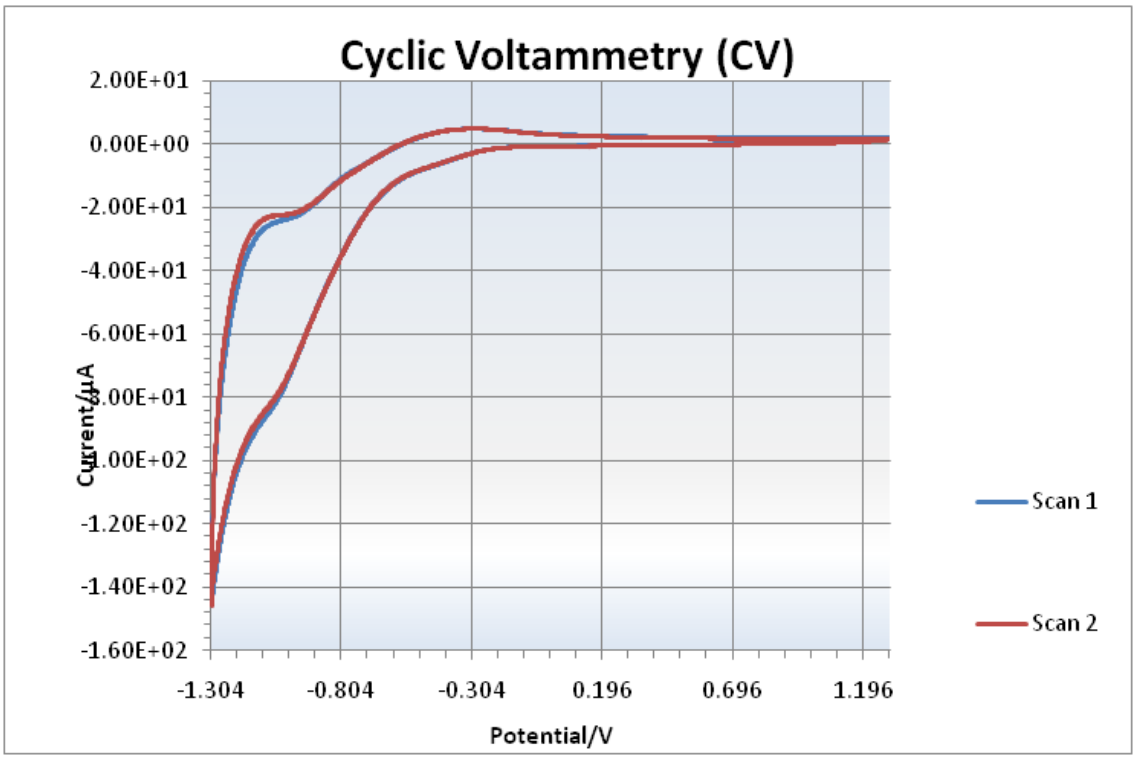

Figure 4.8. CV voltagram of 0.25% Nd doped TiO_2 coated titanium wire.

The Cyclic Voltammetry curves were recorded in Figure 4.8 for 0.25%-Nd doped TiO_2. This doped material was applied on ITO glass by the method of doctor blade. The scan rate was 50mV/s and the applied potential differences were between 1.2V and -1.3V. There were both oxidation-reduction reactions at points -0.9V and -1.1V.

Although the doping per cent was small, distinct curves have formed, meaning interactions, electrochemically. The potentials that have applied was not too large or small.

This voltammogram shows a symmetrical shape indicating that the process is highly reversible so its electrode sample has a capacitance behaviour based on the electrical double layer behaviour principle. The CV shape was not distorted means that TiO_2 layer was strongly adhered on Ti surface. There is no oxide layer breakdown occured of the specific scan rates especially at that scan rate which is 50mV/s for this sample. Even though anodic and cathodic currents have similar shapes, rectangularity was absence. This causes a irreversibility due to the porosity density of the surface because the larger pores increased the current density due to the increased specific surface area for electrical double layer behaviour.

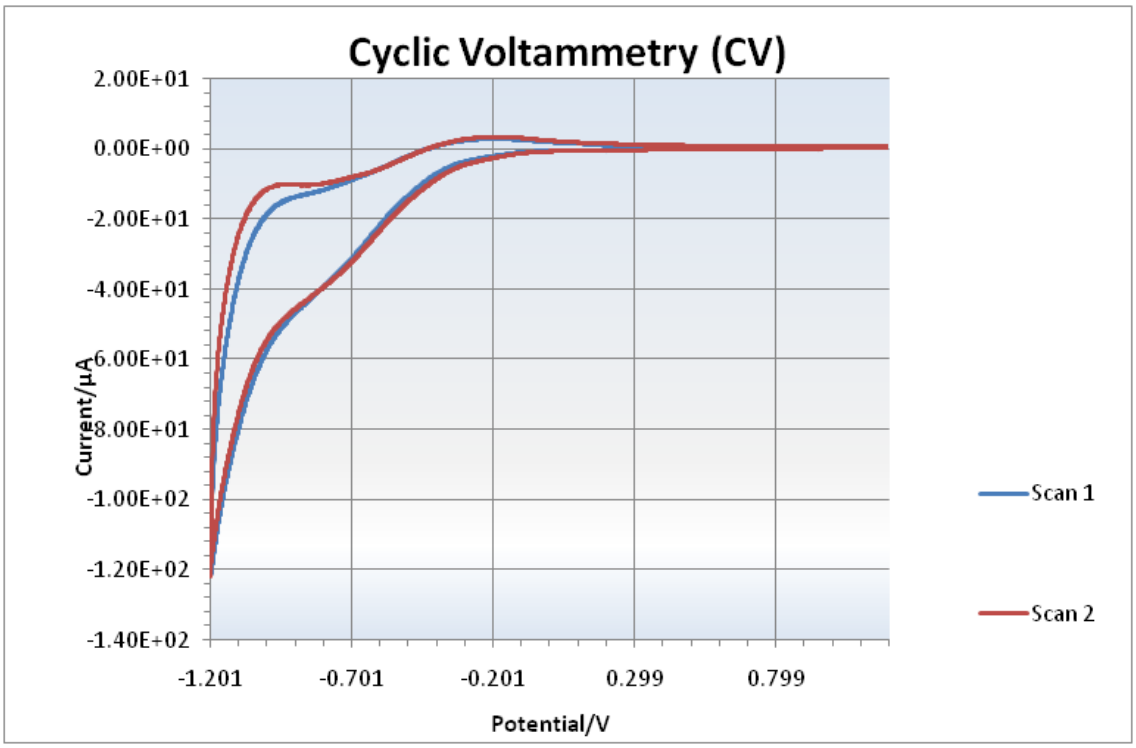

Figure 4.9. CV voltagram of 0.5% Nd doped TiO_2 coated titanium wire.

The Cyclic Voltammetry curves recorded for 0.5% Nd doped TiO_2 in Figure 4.9. As a based material, a six cm height titanium wire was used which immersed into NaOH aqueous solution (CO_2 purged). A potential difference was applied between 0.8V and -1.2V when the scan rate was 50mV/s.

The cathodic peak is seen at -0.2 V where cathodic is realized at -0.8 V. Especially reduction curve seems not sharp because of the technical set of the Palm Sense. Even though scan rate was at the medium levels, potential range is small that means observing distinct wells and hills is almost impossible. As expected, for a little comparison with the Figure 4.3. it is much more definite by the help of interspace.

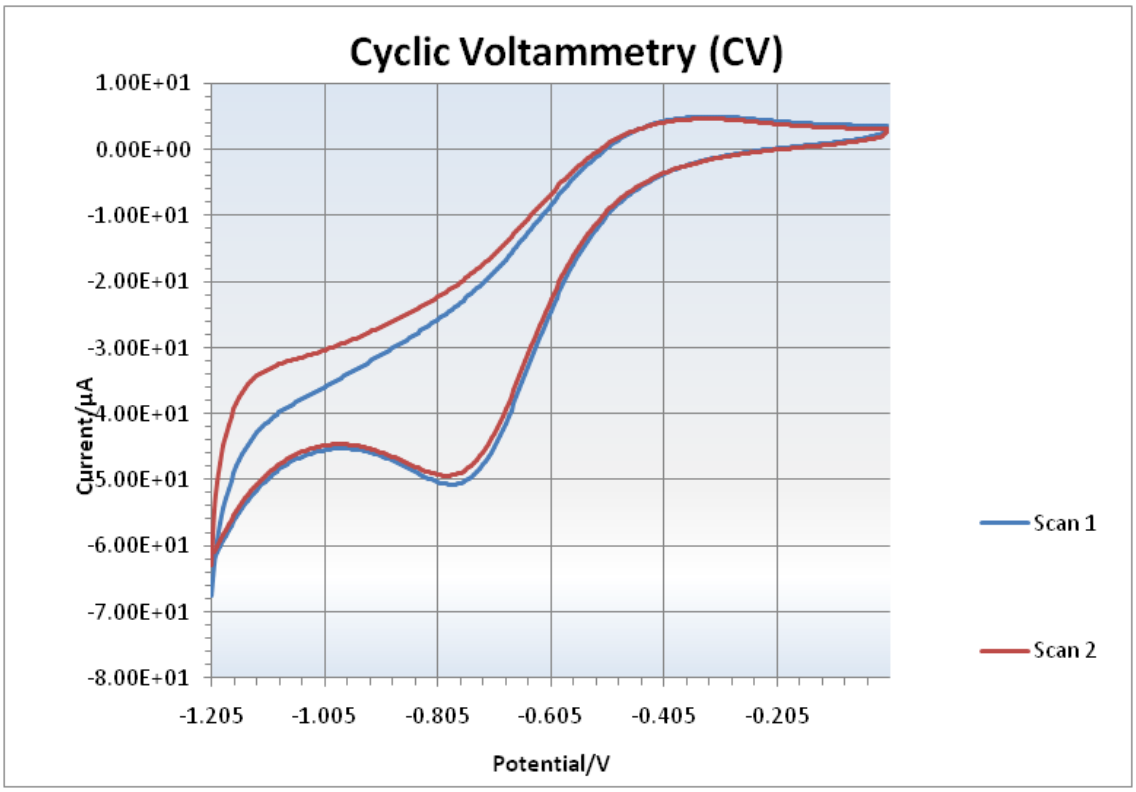

Figure 4.10. CV voltagram of 1% Nd doped TiO_2 coated titanium wire.

The Cyclic Voltammetry curves recorded for 1% Nd doped TiO_2 in Figure 4.10. As a based material, a six cm height titanium wire was used which immersed into NaOH aqueous solution (CO_2 purged). A potential difference was applied between -0.2V and -1.2V when the scan rate was 30mV/s.

A cathodic peak could be observed at -0.35V and an anodic one was seen at -0.75V.

In Figure 4.11. especially reduction seems very sharp and this is mainly caused by Scan Rate. It was samall enough to obtain definite wells. However, at these small scan rates, there could be differences between the first and second runs. It is caused by the some radical ions that were formed during the slow scan.

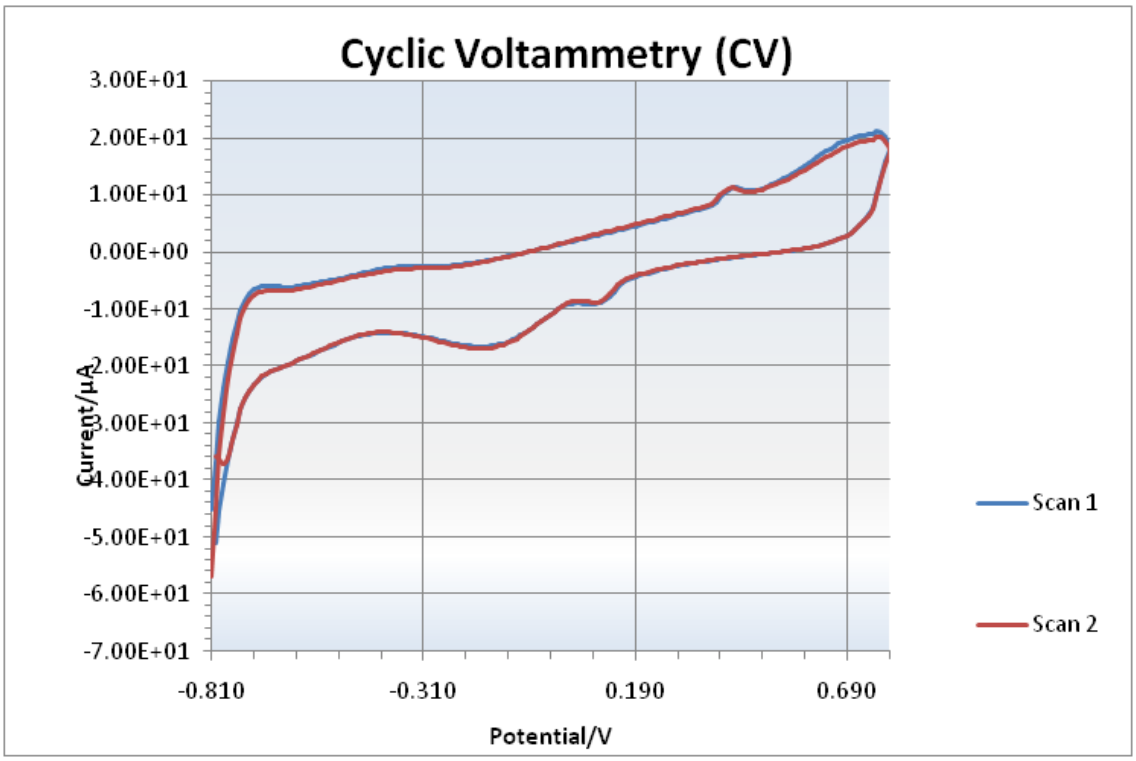

Figure 4.11. CV voltagram of 2% Nd doped TiO_2 coated titanium wire.

The Cyclic Voltammetry curves recorded for 2% Nd doped TiO_2 in Figure 4.11. As a based material, a six cm height titanium wire was used which immersed into NaOH aqueous solution (CO_2 purged). A potential difference was applied between -0.7V and -0.8V when the scan rate was 30mV/s.

A cathodic peak could be observed at 0.45V and an anodic one was seen at 0.1V.

The normative rectangular voltammograms denote the typical electrical double-layer capacitive behaviour. In general, the shape of the CV curve was not typical for titania with two capacitive currents an cathodic region in the case of presence of dopant atoms. Electrochemical reactions occasionally change electronic structure of the titania takes place. This change caused additional energy levels in terms of band gaps which extremely influences the electrical conductivity. The anodic and cathodic peaks as a pair were observed indicating that the origin of the charge storage is reversible faradaic process. These peaks can be matched to the insertion or exertion of alkali cations.

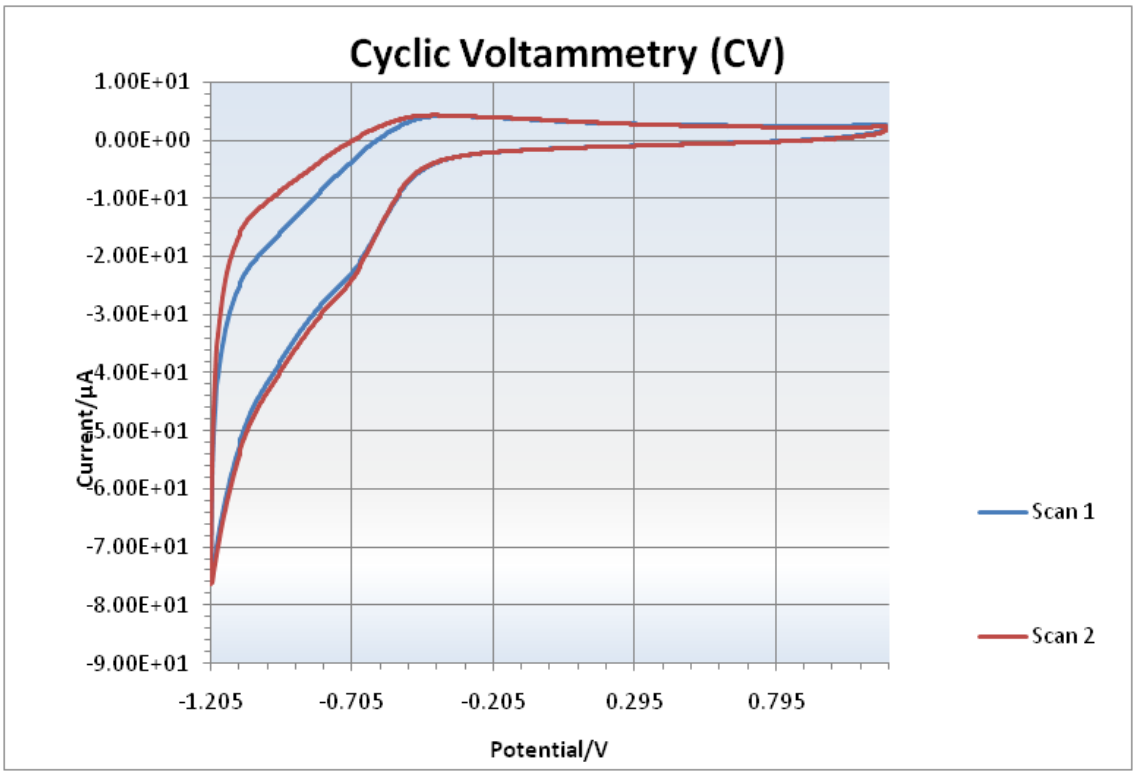

Figure 4.12. CV voltagram of 2% Er doped TiO_2 coated titanium wire.

The Cyclic Voltammetry curves recorded for 2 % Er doped TiO_2 in Figure 4.12. As a based material, a six cm height titanium wire was used which immersed into NaOH aqueous solution (CO_2 purged). A potential difference was applied between -0.7 V and -0.5 V when the scan rate was 60 mV/s.

A cathodic peak could be observed at -0.5 V and an anodic one was seen at -0.7 V.

At this graph, a rectangular shape and reversibility has not been seen. Moreover, unsymmetrical shapes, meaning irreversibility, where stays on the anodic region distorted. It is stated that, the scan rates higher than 30mV/s, due to the oxide surface breakdown and dissolution may lead that peak seperation between first and second runs shown in Figure 4.12 with blue and red lines. It may also caused that, at elevated temperatures, phase transformation or crystallization of titania might take place through grain growth.

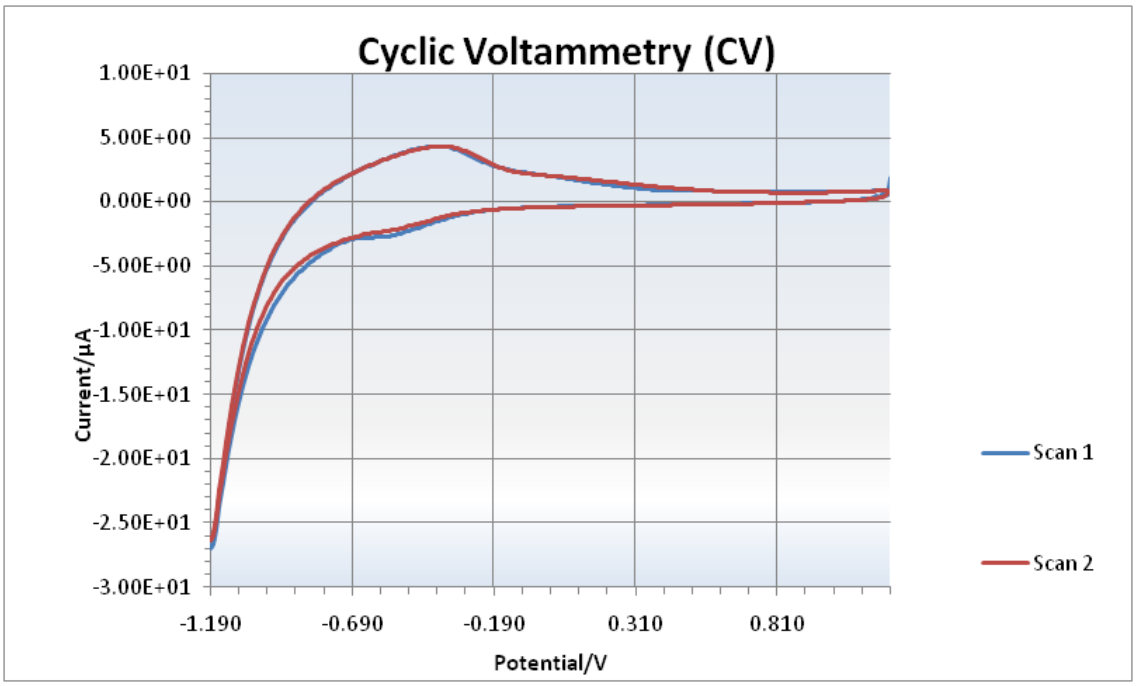

Figure 4.13. CV voltagram of 5% Er doped TiO_2 coated titanium wire

The Cyclic Voltammetry curves recorded for 5 % Er doped TiO_2 in Figure 4.13. As a based material, a six cm height titanium wire was used which immersed into KCl aqueous solution (N purged). A potential difference was applied between -1.2 V and 0.9 V when the scan rate was 40 mV/s.

A cathodic peak could be observed at -0.35V and an anodic one was seen at -0.55 V.

This CV is a typical example of rectangular and symmetrical shape concept. It is emphasized because of its meaning that refers a highly reversible process. Redox peaks were observed so electrode's capacitance behaviour is based on the electrical double layer principle. The voltammogram's shape was not distorded indicating that the oxide layer which might be formed due to oxygen molecules was strictly adhered to Ti surface and no oxide layer breakdown occured at that specific scan rate. It can be expressed that the same reversible characteristic was observed as shown but with higher current density which might indicate the influence of porosity of the surface when a comparison is needed with the Figure 4.12.

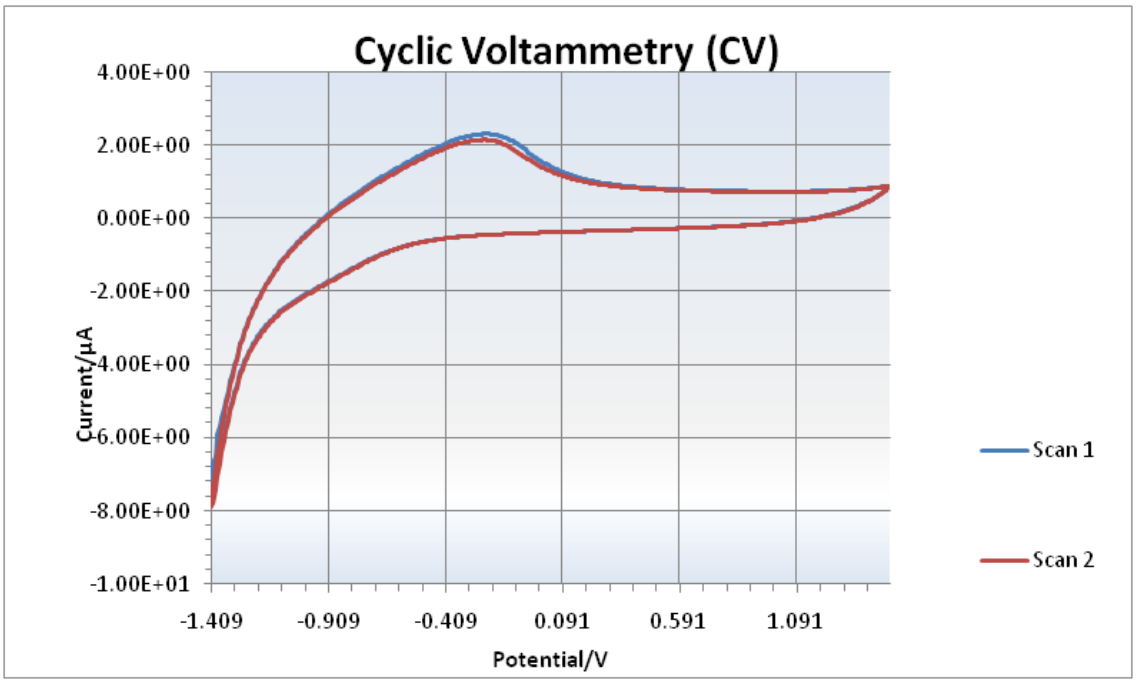

Figure 4.14. CV voltagram of 5% Ce doped TiO_2 coated titanium wire.

The Cyclic Voltammetry curves recorded for 5 % Ce doped TiO_2 in Figure 4.14. As a based material, a six cm height titanium wire was used which immersed into KCl aqueous solution (N purged). A potential difference was applied between -1.5 V and 1.1 V when the scan rate was 50 mV/s.

A cathodic peak could be observed at -0.2V and an anodic one was seen at -0.9 V.

The graph shows the excess current density due to the addition of Ce atoms into the titania based sol. The cathodic peak, within a normal scan rate level, shifted towards slightly less positive potentials as a bump compared to 5 % Er doped in Figure 4.13. The current associated with that peak became more negative with a closer look at the behaviour of this peak. In addition, it is assumed that the charge involved during the oxidation-reduction reactions were mainly due to the titania molecules in which formed as a layer on the wire. Since, there is no significant response corresponding to titania oxidation-reduction where could be observed within the potential scan range. It is noted that, during the cathodic potential scan, the onset of oxidation shifted toward more positive potential as the amount of coated titania density.

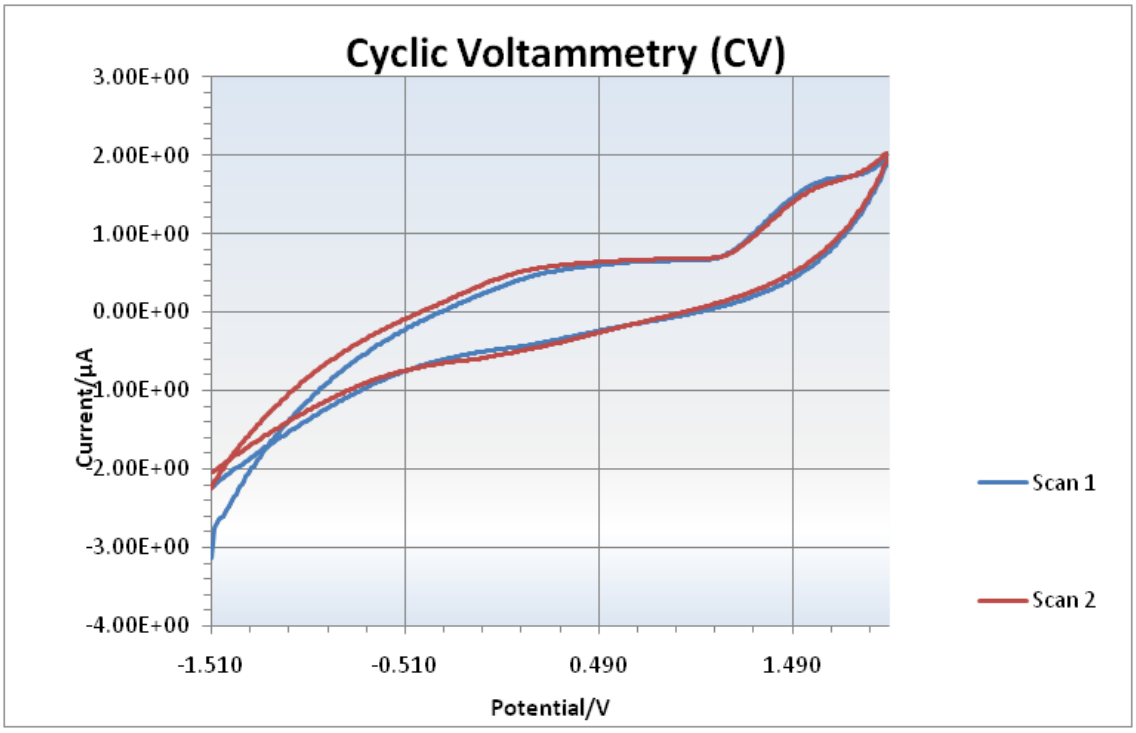

Figure 4.15. CV voltagram of 5% La doped TiO_2 coated titanium wire.

The Cyclic Voltammetry curves recorded for 5 % La doped TiO_2 in Figure 4.15. As a based material, a six cm height titanium wire was used which immersed into KCl aqueous solution (N purged). A potential difference was applied between -1.5 V and 1.1 V when the scan rate was 50 mV/s.

A cathodic peak could not be observed. From the voltammograms, no redox peaks were observed at that scan rate meaning therefore the electrode shows double layer capacitance behaviour. In the literature, it is noted that the CVs at scan rates higher than 30mV/s was due to a oxide surface breakdown and dissolution which had been caused. It is also added that if a CV measurement with an increase in the current density at oxidation expected regions shows no peaks due to the pitting corrision.

Finally, direct and reverse potentials, in other words, anodic and cathodic currents was not shown which can be perturbed by OH^- anions explained by the pH change.

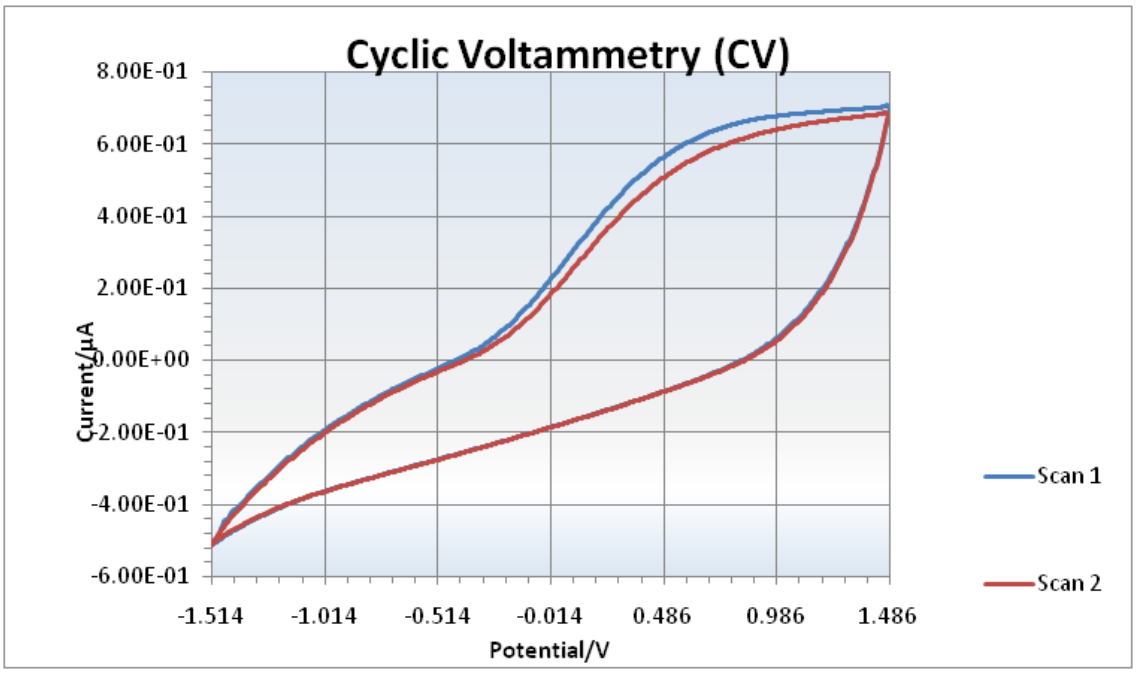

Figure 4.16. CV voltagram of 5% Ce doped TiO_2 coated titanium wire.

The Cyclic Voltammetry curves recorded for 10 % Ce doped TiO_2 in Figure 4.16. As a based material, a six cm height titanium wire was used which immersed into KCl aqueous solution (N purged). A potential difference was applied between -1.5 V and 1.1 V when the scan rate was 100 mV/s.

A cathodic peak could not be observed.

In figure 4.17, the CV measurements were tried to plot different scan rates of a same pristine TiO_2 sample is performed and overlapping voltammograms are drawn within the illustration program called “Origin”. Colours; black, red, blue and green refer to the scan rates as 0.03, 0.05, 0.07 and 0.09 V/s respectively. 0.1M KCl aqueous solution was used N_2 is purged sufficiently.

The working electrode was polarized from rest potential in the anodic direction up to 1.5V and back up -1.3V. In academic literature the shapes of CV curves are typical for titanium dioxide materials with a marginal capacitive anodic current.

Furthermore, the area surrounded by the CV curves for the pristine sample is determining. It is apparently seen that the black voltammogram occupys the larger area with 30mV/s. However, in the CV papers, it is depicted and defined the faster the rate, the larger the surrounded area. It may be occurred due to the effects of the crystal defects caused by the impurities which is mainly meaned resistance of the electrode. It can also

noted that with an increase in scan rate especially with blue and green lines, a negative shift of reduction peaks were observed.

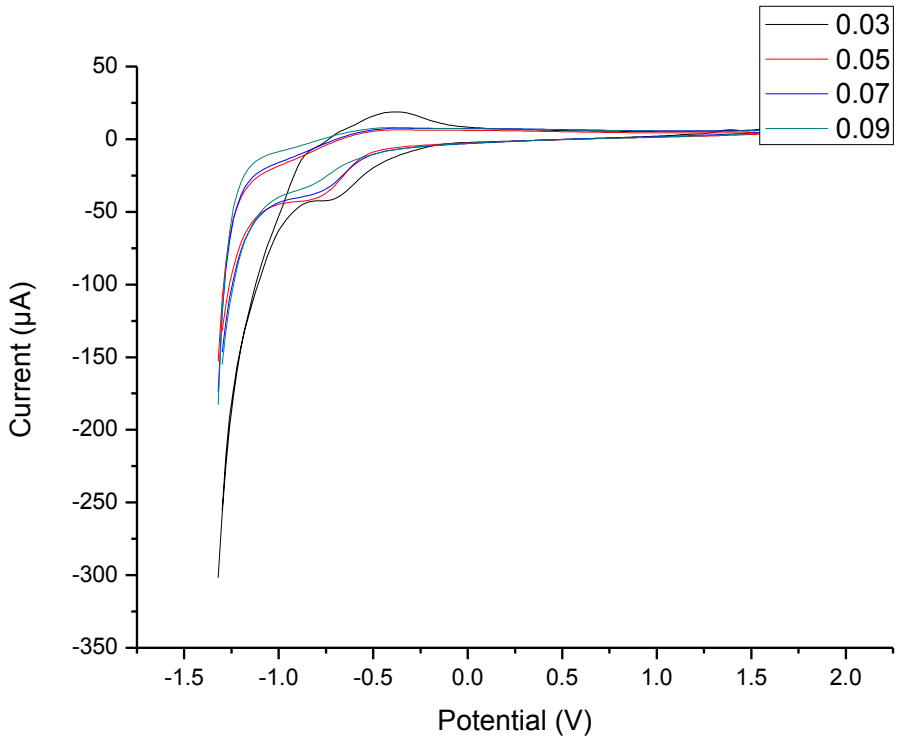

Figure 4.17 Voltammograms of Pristine TiO_2 with various scan rates.

In the illustrations, differences due to the scan rates could be observed and the relation between the integrated area and the speed of scans were realized consistently.

Results of the pristine sample was encourager so they were tried again. However, this time a doped sample was used for 6 different scan rates. In Figure 4.18, these scan rates were run and results were drawn. The integrated area of the curves change due to the speed of the scans which differ from 20mV/s to 80mV/s. The reason why % 0.5 Nd doped sample was used during this measurement was to compare with pristine sample and doped one. Doping seems might cause extra crystal defects effecting the resistance somehow. In this figure the voltammogram at a scan rate 50 mV/s with the red line seems the exception of the estimation that claims the faster the scan, the larger the surrounded area. As it is mentioned before, doping might lead this kind of diversity by already having crystal defects.

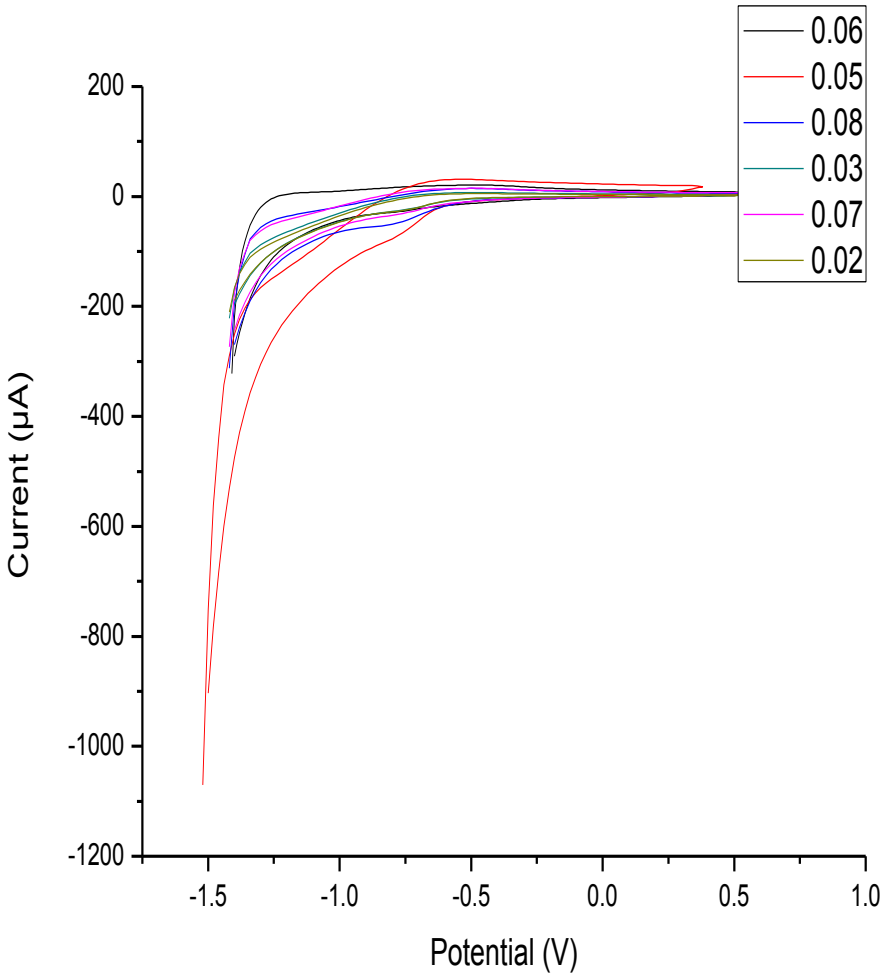

Figure 4.18 Voltammograms of 0.5 Nd doped TiO_2 with various scan rates.

To understand how doping atoms influences the measurement another concept was planned within controlled experiments. In Figure 4.19, three different voltammograms were drawn to find out difference between doping elements in same conditions which are in 0.1M aqueous solution, applied same potential difference. In order to evaluate the electrochemical properties of the electrode materials and those CV tests are employed at 50mV/s to characterize the capacitance of performances. The normative rectangular CV curves denote the typical electrical double-layer capacitive behavior.

In addition, comparison of the areas surrounded by the CV curve of %1Nd doped one apperantly larger than the other at the same scan rate which indicates much more improved specific capacitance. La doped is negligibly smaller than Ce doped which means probably resulting from the higher surface area and the enhanced accesibility by electrolyte ions.

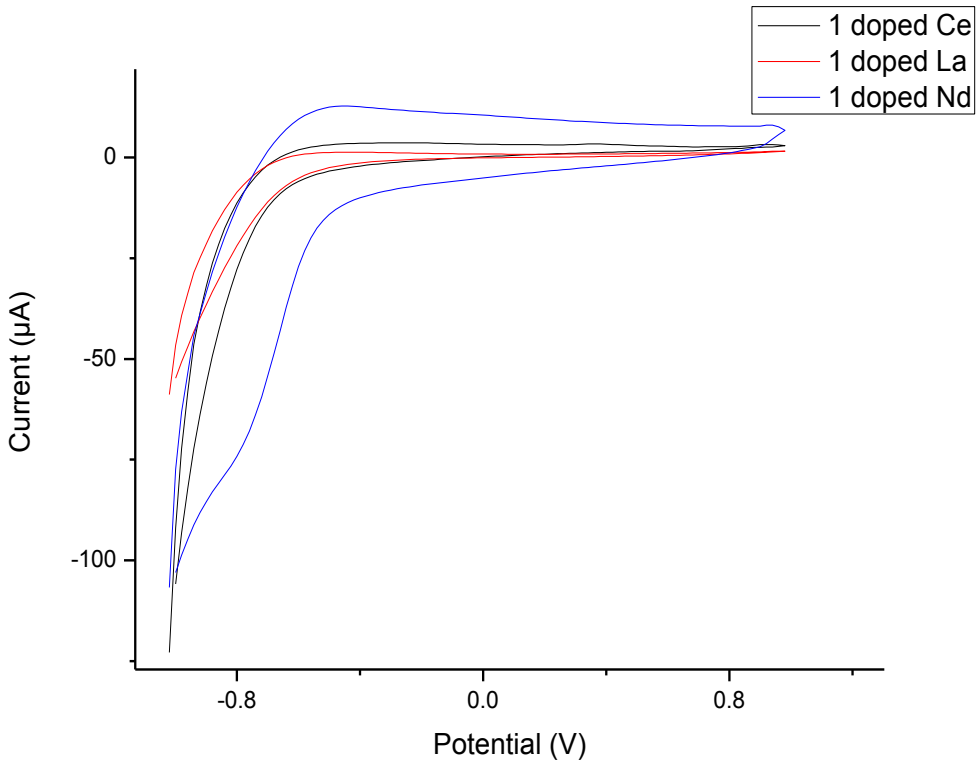

Figure 4.19 Voltammograms of % 1 Ce, La and Nd doped TiO_2 samples

Working with electrodes needs new ideas and methods to control the whole experiment. Measurement technique might directly influences the analysis. During the analysis a confusion leaded the methods about how surface area influences the measurements. Whether a difference was occurred due to the amount of dipped wire or not was one of the main question. In order to evaluate this problem, measurements were renewed by using the wires as pairs. These two wires were kept by the crocodile and the whole method was applied on them. In Figure 4.20, pair wires and single ones were both dipped into the solution and results were different eachother as expected. The difference of the plots could easily be isolated because reached minimum current density was completely different although the the difference between the runs as 50mV and 70mV.

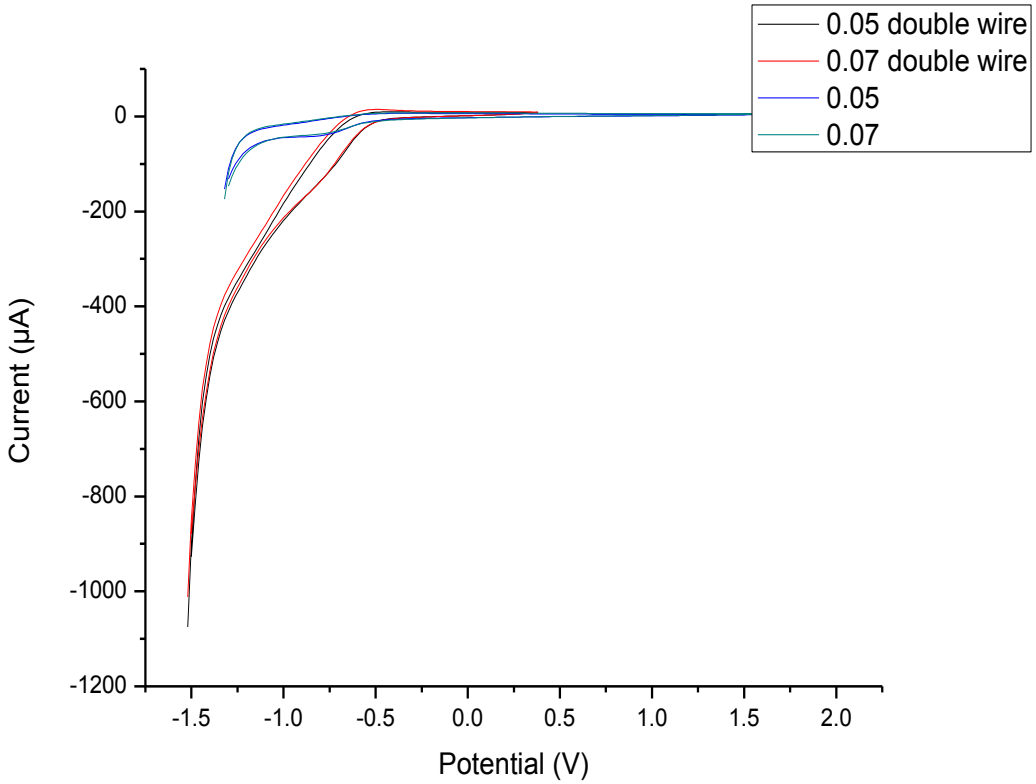

Figure 4.20 Voltammograms of pure TiO_2 samples with 50mV/s and 70mV/s to compare surface areas of single and pair wires

Double wire plots which were represented by the red and black lines reached approximately -1100 μA whereas the single ones were at -200 μA. This might show that improved accessibility by electrolyte ions could be controlled by surface area of the electrodes.

CHAPTER 5

CONCLUSION

The graphs mainly showed that lots of results can be seen from the partial behaviours of electrochemical interactions. Dark environment was accepted essential for the measurements to not influence them. Sample characterization could be done like with the methods that had been tried, responses of them could be plotted and compared. Ensurance of each level of this experiment system could be possible with the views of the microscobic data and figures. Some eleminations were realized randomly, nevertheless, other fundemental issues were became real as expected before experimental initiation. The redox reactions of selected doped TiO_2 samples were examined under various conditions. The results obtained indicate that their electrochemical features were affected by the kind and nature of the working electrode used, as well as the doping type under investigation. After the misuse of doctor-blade method and disadventagous results, separate oxidation and reduction peaks were observed. Multiple oxidation peaks were detected on the titania electrodes for especially Nd doped ones. Furthermore in comparison graphs it was proved that Nd atoms were much more active than the other dopants those were used during other intents. Based on these findings, this could be seen that associating the oxidation-reduction peaks of these electrodes to a single potential could not be definitely depict the situation. It depended on the type of working electrode being prepared.

The basic aim was to show the relation between the electrochemical activity and the doping style and Cyclic Voltammetry working styles were studied, tried and compared. Installation and its principles were tested on a number of occasions. Other important goals were also reached as oxidation reduction results which will be used in the future for redox potentials and the band gap calculation. Moreover scan rate comparisons were done to compare electron transfer speed of electrolyte ions. In another multiple graph, doping type was explicated and Nd was the winner when the topic was activity. To understand how surface area affects the electron transfer, all system was prepared again for the double wire experiment. Results were not unexpected. The whole work was finished to be used in the future as guide to whom it may benefit during artificial photosynthesis and band gap researches on the way of CV.

REFERENCES

Akpan, U., Hameed, B., 2010. The advancements in sol–gel method of doped-TiO 2 photocatalysts. Applied Catalysis A: General 375, 1-11.

Baiju, K., Periyat, P., Wunderlich, W., Pillai, P. K., Mukundan, P., Warrier, K., 2007. Enhanced photoactivity of neodymium doped mesoporous titania synthesized through aqueous sol–gel method. Journal of sol-gel science and technology 43, 283-290.

Carp, O., Huisman, C. L., Reller, A., 2004. Photoinduced reactivity of titanium dioxide. Progress in solid state chemistry 32, 33-177.

Choudhury, B., Borah, B., Choudhury, A., 2013. Ce–Nd codoping effect on the structural and optical properties of TiO 2 nanoparticles. Materials Science and Engineering: B 178, 239-247.

Cogdell, R. J., Brotosudarmo, T. H., Gardiner, A. T., Sanchez, P. M., Cronin, L., 2010. Artificial photosynthesis–solar fuels: current status and future prospects. Biofuels 1, 861-876.

Cong, Y., Zhang, J., Chen, F., Anpo, M., 2007. Synthesis and characterization of nitrogen-doped TiO2 nanophotocatalyst with high visible light activity. The Journal of Physical Chemistry C 111, 6976-6982.

Cardoso L. M., Mainier F. B., Itabirano J. A. P. 2014. Analysis Voltammetry of Cyanide and Process Electrolytic Removal of Cyanide in Effluents. American Journal of Environmental Engineering, 4(6): 182-188.

Crystal structures of titania, 2015. http://imgbuddy.com/tio2-structure.asp

Cyclic Voltammetry, 2015. https://www.basinc.com/library/cvnotes/.

Dey, G., 2007. Chemical reduction of CO 2 to different products during photo catalytic reaction on TiO 2 under diverse conditions: an overview. Journal of natural gas chemistry 16, 217-226.

DuVall, S. H., McCreery, R. L., 1999. Control of catechol and hydroquinone electron-transfer kinetics on native and modified glassy carbon electrodes. Analytical Chemistry 71, 4594-4602.

Electrochemical photoreduction, 2015. http://wws.weizmann.ac.il/Organic_Chemistry/ neumann/photoreduction-carbon-dioxide

Fan, Y., Li, D., Deng, M., Luo, Y., Meng, Q., 2009. An overview on water splitting photocatalysts. Frontiers of Chemistry in China 4, 343-351.

Fatin, S., Lim, H., Tan, W., Huang, N., 2012. Comparison of photocatalytic activity and cyclic voltammetry of zinc oxide and titanium dioxide nanoparticles toward degradation of methylene blue. International Journal of Electrochemical Science 7, 9074-9084.

Fujishima, A., 1972. Electrochemical photolysis of water at a semiconductor electrode. nature 238, 37-38.

Hammarström, L., Hammes-Schiffer, S., 2009. Artificial photosynthesis and solar fuels. Accounts of chemical research 42, 1859-1860.

Heldt, H., 2005. The use of energy from sunlight by photosynthesis is the basis of life on earth. Plant Biochemistry 3, 56-58.

Huang., Gan,. M., Ma,. L,. Yu,. Hu,. Yang,. Li,. Chengqiang,. 2015. Fabrication of polyaniline/graphene/titania nanotube arrays nanocomposite and their application in supercapacitors

Hoffmann, M. R., Martin, S. T., Choi, W., Bahnemann, D. W., 1995. Environmental applications of semiconductor photocatalysis. Chemical reviews 95, 69-96.

Huskinson B., Marshak M. P., Suh C., Er S., Gerhardt M. R. , Galvin C. J. , Chen X., Aspuru-Guzik A, Gordon R. G., Aziz M. J. A. 2014. Metal-free organic–inorganic aqueous flow battery, Nature 505, 195–198.

Inoue, T., Fujishima, A., Konishi, S., Honda, K., 1979. Photoelectrocatalytic reduction of carbon dioxide in aqueous suspensions of semiconductor powders. Nature 277, 637-638.

Inoue, Y., 2009. Photocatalytic water splitting by RuO 2-loaded metal oxides and nitrides with d 0-and d 10-related electronic configurations. Energy & Environmental Science 2, 364-386.

Kalyanasundaram, K., Graetzel, M., 2010. Artificial photosynthesis: biomimetic approaches to solar energy conversion and storage. Current opinion in Biotechnology 21, 298-310.

Kiesgen de_Richter, R., Ming, T., Caillol, S., 2013. Fighting global warming by photocatalytic reduction of CO 2 using giant photocatalytic reactors. Renewable and Sustainable Energy Reviews 19, 82-106.

Kočí, K., Obalová, L., Matějová, L., Plachá, D., Lacný, Z., Jirkovský, J., Šolcová, O., 2009. Effect of TiO 2 particle size on the photocatalytic reduction of CO 2. Applied Catalysis B: Environmental 89, 494-502.

Kudo, A., Miseki, Y., 2009. Heterogeneous photocatalyst materials for water splitting. Chemical Society Reviews 38, 253-278.

Labouriau, A., Earl, W. L., 1997. Titanium solid-state NMR in anatase, brookite and rutile. Chemical physics letters 270, 278-284.

Li, F., Li, X., Hou, M., 2004. Photocatalytic degradation of 2-mercaptobenzothiazole in aqueous La 3+–TiO 2 suspension for odor control. Applied Catalysis B: Environmental 48, 185-194.

Linsebigler, A. L., Lu, G., Yates Jr, J. T., 1995. Photocatalysis on TiO2 surfaces: principles, mechanisms, and selected results. Chemical reviews 95, 735-758.

Lou, S., Teng, F., Xu., J., Zhu., 2015. Electrochemical Properties of Novel Titania Nanostructures

Löberg, J., Perez Holmberg, J., Mattisson, I., Arvidsson, A., Ahlberg, E., 2013. Electronic Properties of Nanoparticles Films and the Effect on Apatite-Forming Ability. International journal of dentistry 2013.

Matějová, L., Kočí, K., Reli, M., Čapek, L., Hospodková, A., Peikertová, P., Matěj, Z., Obalová, L., Wach, A., Kuśtrowski, P., 2014. Preparation, characterization and photocatalytic properties of cerium doped TiO 2: On the effect of Ce loading on the photocatalytic reduction of carbon dioxide. Applied Catalysis B: Environmental 152, 172-183.

Marin Mineral, 2015. http://www.marinmineral.com/anatase.html

Mineral MasterPiece, 2015. http://www.mineralmasterpiece.com/Sold_Specimen_p7

Mu, J., Chen, B., Zhang, M., Guo, Z., Zhang, P., Zhang, Z., Sun, Y., Shao, C., Liu, Y., 2011. Enhancement of the visible-light photocatalytic activity of In2O3–TiO2 nanofiber heteroarchitectures. ACS applied materials & interfaces 4, 424-430.

Nassoko, D., Li, Y.-F., Li, J.-L., Li, X., Yu, Y., 2012. Neodymium-Doped with Anatase and Brookite Two Phases: Mechanism for Photocatalytic Activity Enhancement under Visible Light and the Role of Electron. International Journal of Photoenergy

Neațu, Ș., Maciá-Agulló, J. A., Garcia, H., 2014. Solar light photocatalytic CO2 reduction: general considerations and selected bench-mark photocatalysts. International journal of molecular sciences 15, 5246-5262.

Nello Formisano, Pawan Jolly, Mary Cromhout, Shane Flanagan, Ronen Fogel, Janice L Limson, Pedro Estrela; 2015. Optimisation of an Electrochemical Impedance Spectroscopy aptasenor by exploiting Quartz Crystal Microbalance with Dissipation Signals. 220, 369-375.

Nie, X., Zhuo, S., Maeng, G., Sohlberg, K., 2009. Doping of T i O 2 Polymorphs for Altered Optical and Photocatalytic Properties. International Journal of Photoenergy.

Nicholson, R. S. Irving. Shain 1964. Theory of Stationary Electrode Polarography Single Scan and Cyclic Methods Applied to Reversible, Irreversible and Kinetic Systems. Analytical Chemistry.

Obregón, S., Kubacka, A., Fernández-García, M., Colón, G., 2013. High-performance Er 3+–TiO 2 system: Dual up-conversion and electronic role of the lanthanide. Journal of Catalysis 299, 298-306.

Oxidation and Reduction Process, 2015. http://www.engr.uconn.edu/jmfent/CHEG320_ electrochemistry.pdf)

Park, J. H., Kim, S., Bard, A. J., 2006. Novel carbon-doped TiO2 nanotube arrays with high aspect ratios for efficient solar water splitting. Nano letters 6, 24-28.

Raja, K., Smith, Y., Kondamudi, N., Manivannan, A., Misra, M., Subramanian, V. R., 2011. CO2 photoreduction in the liquid phase over Pd-supported on TiO2 nanotube and bismuth titanate photocatalysts. Electrochemical and Solid-State Letters 14, F5-F8.

Ranjit, K., Willner, I., Bossmann, S., Braun, A., 2001. Lanthanide oxide-doped titanium dioxide photocatalysts: novel photocatalysts for the enhanced degradation of p-chlorophenoxyacetic acid. Environmental science & technology 35, 1544-1549.

René McCormick, 2006. Reduction process of basic ions and molecules, College Board

Rockafellow, E. M., Stewart, L. K., Jenks, W. S., 2009. Is sulfur-doped TiO 2 an effective visible light photocatalyst for remediation? Applied Catalysis B: Environmental 91, 554-562.

Petrucci et al. 2007. General Chemistry: Principles and Modern Applications. 9th ed. Upper Saddle River, New Jersey: Pearson Education.

Shen, H., Mi, L., Xu, P., Shen, W., Wang, P.-N., 2007. Visible-light photocatalysis of nitrogen-doped TiO 2 nanoparticulate films prepared by low-energy ion implantation. Applied Surface Science 253, 7024-7028.

Silija, P., Yaakob, Z., Suraja, V., Binitha, N. N., Akmal, Z. S., 2011. An enthusiastic glance in to the visible responsive photocatalysts for energy production and pollutant removal, with special emphasis on titania. International Journal of Photoenergy 2012.

Siuzdak, K., Szkoda, M., Sawczak, M., Lisowska-Oleksiak, A., Karczewski, J., Ryl, J., 2015. Enhanced photoelectrochemical and photocatalytic performance of iodine-doped titania nanotube arrays. RSC Advances 5, 50379-50391.

Solar cell, 2008. http://teachers.usd497.org/agleue/Gratzel_solar_cell%20assets/ How%20does%20a%20Gratzel%20Solar%20Cell%20work.htm

Tahir, M., Amin, N. S., 2013. Recycling of carbon dioxide to renewable fuels by photocatalysis: Prospects and challenges. Renewable and Sustainable Energy Reviews 25, 560-579.

Tan, J. Z., Fernández, Y., Liu, D., Maroto-Valer, M., Bian, J., Zhang, X., 2012. Photoreduction of CO 2 using copper-decorated TiO 2 nanorod films with localized surface plasmon behavior. Chemical Physics Letters 531, 149-154.

Uner, D., Oymak, M. M., İpek, B., 2011. CO 2 utilisation by photocatalytic conversion to methane and methanol. International Journal of global warming 3, 142-162.

World Consumption, 2006. www.edro.wordpress.com.

Wu, G., Chen, T., Su, W., Zhou, G., Zong, X., Lei, Z., Li, C., 2008. H 2 production with ultra-low CO selectivity via photocatalytic reforming of methanol on Au/TiO 2 catalyst. International Journal of Hydrogen Energy 33, 1243-1251.

Wu, Y., Lu, G., Li, S., 2006. The long-term photocatalytic stability of Co 2+-modified P25-TiO 2 powders for the H 2 production from aqueous ethanol solution. Journal of Photochemistry and Photobiology A: Chemistry 181, 263-267.

Xiao, Q., Si, Z., Zhang, J., Xiao, C., Tan, X., 2008. Photoinduced hydroxyl radical and photocatalytic activity of samarium-doped TiO 2 nanocrystalline. Journal of Hazardous materials 150, 62-67.

Yang, G., Jiang, Z., Shi, H., Xiao, T., Yan, Z., 2010. Preparation of highly visible-light active N-doped TiO 2 photocatalyst. Journal of Materials Chemistry 20, 5301-5309.

Zaleska, A., 2008. Doped-TiO2: a review. Recent Patents on Engineering 2, 157-164.

Zang, L., 2011. Energy Efficiency and Renewable Energy Through Nanotechnology. Springer.

Zhang, Q.-H., Han, W.-D., Hong, Y.-J., Yu, J.-G., 2009. Photocatalytic reduction of CO 2 with H 2 O on Pt-loaded TiO 2 catalyst. Catalysis Today 148, 335-340.

Zhu, J., Zäch, M., 2009. Nanostructured materials for photocatalytic hydrogen production. Current Opinion in Colloid & Interface Science 14, 260-269.